Structural Characterization of Membrane Proteins and Peptides by FTIR and ATR-FTIR Spectroscopy

ARTICLE *in* METHODS IN MOLECULAR BIOLOGY (CLIFTON, N.J.) · FEBRUARY 2013

Impact Factor: 1.29 · DOI: 10.1007/978-1-62703-275-9_9 · Source: PubMed

1 AUTHOR:

Suren Tatulian
University of Central Florida
85 PUBLICATIONS **2,275** CITATIONS

Chapter 9

Structural Characterization of Membrane Proteins and Peptides by FTIR and ATR-FTIR Spectroscopy

Suren A. Tatulian

Abstract

Fourier transform infrared (FTIR) spectroscopy is widely used in structural characterization of proteins or peptides. While the method does not have the capability of providing the precise, atomic-resolution molecular structure, it is exquisitely sensitive to conformational changes occurring in proteins upon functional transitions or upon intermolecular interactions. Sensitivity of vibrational frequencies to atomic masses has led to development of "isotope-edited" FTIR spectroscopy, where structural effects in two proteins, one unlabeled and the other labeled with a heavier stable isotope, such as ^{13}C, are resolved simultaneously based on spectral downshift (separation) of the amide I band of the labeled protein. The same isotope effect is used to identify site-specific conformational changes in proteins by site-directed or segmental isotope labeling. Negligible light scattering in the infrared region provides an opportunity to study intermolecular interactions between large protein complexes, interactions of proteins and peptides with lipid vesicles, or protein–nucleic acid interactions without light scattering problems often encountered in ultraviolet spectroscopy. Attenuated total reflection FTIR (ATR-FTIR) is a surface-sensitive version of infrared spectroscopy that has proved useful in studying membrane proteins and lipids, protein-membrane interactions, mechanisms of interfacial enzymes, and molecular architecture of membrane pore or channel forming proteins and peptides. The purpose of this article was to provide a practical guide to analyze protein structure and protein-membrane interactions by FTIR and ATR-FTIR techniques, including procedures of sample preparation, measurements, and data analysis. Basic background information on FTIR spectroscopy, as well as some relatively new developments in structural and functional characterization of proteins and peptides in lipid membranes, are also presented.

Key words: Infrared spectroscopy, Protein structure, Lipid structure, Membrane, Protein-membrane interactions, Transmembrane orientation, Protein isotope labeling

1. Introduction

FTIR spectroscopy has become one of the most popular techniques employed in structural characterization of proteins and peptides. The utility of this method is based, first of all, on the wide spectral range of a single spectrum, which covers the vibrational frequencies of various chemical groups occurring not only in a polypeptide

Jörg H. Kleinschmidt (ed.), *Lipid-Protein Interactions: Methods and Protocols*, Methods in Molecular Biology, vol. 974,
DOI 10.1007/978-1-62703-275-9_9,

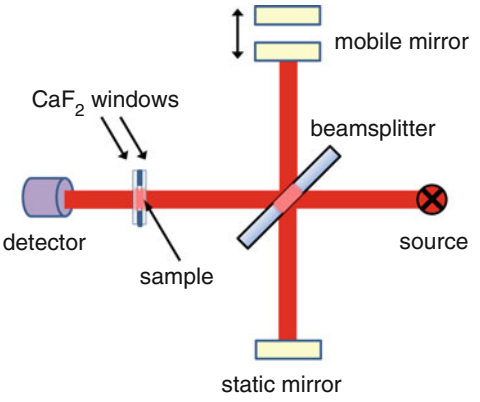

Fig. 1. Schematic presentation of the infrared experimental setup. Description is provided in the main text.

chain but practically in all organic and inorganic compounds. This allows for analysis of interactions of proteins with lipids, nucleic acids, drugs, and other molecules; the spectra of complex systems provide structural information on all components that generate absorbance bands at specific spectral regions. Moreover, since various structural or functional groups of biomolecules have distinct chemical compositions and hence absorb at specific frequencies, information on the individual functional groups of molecules is obtained from FTIR spectra without the need of labeling with molecular probes. Other advantages of FTIR spectroscopy include the absence of light scattering problems, often encountered in UV spectroscopy such as circular dichroism or fluorescence. This is especially important when working with membrane proteins or peptides in the presence of lipid vesicles, which strongly scatter at lower wavelengths in the UV region. The kinetics of amide hydrogen/deuterium exchange (HX) of a protein upon exposure to D_2O is readily measured by FTIR and provides information on the structural flexibility and the degree of solvent accessibility, that is, the structural dynamics of proteins. Polarized ATR-FTIR offers additional advantages such as increased sensitivity and an opportunity to determine the orientation of membrane-bound proteins in addition to their secondary structure and dynamic properties. Sensitivity of infrared vibrations to atomic masses allows one to gain site-specific structural information on proteins by stable isotope labeling, without gross perturbations like those often induced by labeling with relatively bulky chemical groups. Lastly, the ease of FTIR experiments and the affordable cost of instrumentation make it a facile yet powerful technique for protein structural studies.

FTIR instrumentation is relatively simple (Fig. 1). The infrared light source, such as a heated tungsten filament, radiates polychromatic light in the infrared region. The beam is directed to a Michelson interferometer that contains a beam splitter, for

example, germanium, which passes 50 % of the beam and reflects the other 50 %. The split beams hit two mirrors, one static and the other oscillating back and forth with certain frequency and amplitude. The two beams, reflected from the static and mobile mirrors, recombine at the beam splitter, undergo interference because of the optical path-length difference (Δl), and travel to the sample. In direct transmission FTIR, the sample is normally placed between two infrared-transparent windows, such as CaF_2, separated by a thin (typically 5–50 μm) spacer. The beam passes through the sample and travels to the detector, such as a high-sensitivity, liquid nitrogen-cooled Hg/Cd/Te (MCT) detector, which simply records the light intensity. For each individual wavelength within the beam, the beams returning from the static and mobile mirrors undergo constructive interference at zero Δl as well as constructive or destructive interference at $\Delta l = m\lambda$ or $\Delta l = (m + 1/2)\lambda$, respectively, where m is any integral number. The result is that the light that reaches the detector is a sum of cosine functions, known as the interferogram. Fourier transformation of the interferogram results in a transmission spectrum, that is, the intensity of transmitted light as a function of frequency (or the wavenumber). (The wavenumber is $W = 1/\lambda = v/c$, where λ is the wavelength, v is the temporal frequency of the vibration, and c is the speed of light.) The resolution of the spectrum is directly proportional to the total displacement of the mobile mirror, so at a constant speed of the mobile mirror, collection of higher resolution spectra (such as ~1 cm^{-1}) will take longer time. Also, the quality (i.e., the signal-to-noise ratio) is proportional to $\sqrt{N}$, where N is the number of scans per spectrum, so again recording of a "good" spectrum will take longer time. (Normally, 1,000 scans can be collected in ~15 min) When two transmission spectra are recorded, one for the (protein) sample and the other for the blank buffer or any other "reference," the absorbance spectrum is calculated either automatically or manually as $A = -\lg(T_s/T_r)$, where T_s and T_r are the transmissions of the sample and the reference, respectively.

A polypeptide chain generates several infrared-active amide vibrational modes (Table 1), among which the amide I and amide II modes have been analyzed most extensively because of their exceptional sensitivity to the secondary structure and the kinetics of HX, respectively. Both are delocalized vibrational modes and include contributions from various chemical bonds within the amide group. The amide I mode occurs between 1,700 and 1,600 cm^{-1} and is generated primarily by the C=O stretching vibration, plus CN and CCN out-of-plane bending vibrations and minimally by the NH in-plane bending mode (1). The resulting amide I oscillators are coupled to each other via covalent bonds, H-bonding, and through space, all of which are distinct for different secondary structures (1, 2). Consequently, different secondary structures of polypeptides produce amide I bands at distinct

Table 1
Description of various amide vibrational modes and the wavenumbers (W) in H_2O and D_2O[a]

Amide mode	W_{H2O} (cm^{-1})	W_{D2O} (cm^{-1})	Approximate contributions from individual chemical bonds (%)[b]
Amide I	1,700–1,600	1,700–1,600[c]	CO s (76), CN s (11), CCN d (8), NH ib (5)
Amide II	1,570–1,540	1,480–1,460	NH ib (45), CN s (30), CO ib (10) CC s (8), NC s (7)
Amide III	~1,250	~960	NH ib (50), CC s (20), CN s (18), CO ib (12)
Amide IV	640–620	640–620[c]	CO ib (45), CC s (35), CNC d (20)
Amide V	735–715	520–500	CN t (62), NH ob (38)
Amide VI	650–600	650–600[c]	CO ob (85), CN t (15)
Amide VII	230–200	165–150	NH ob (68), CN t (20), CO ob (12)
Amide A	~3,300	2,500–2,400	Fermi resonance between NH s and amide II
Amide B	3,100–3,050	~2,400	Fermi resonance between NH s and amide II

[a]Adapted from refs. (1, 102)
[b]s, stretching; d, deformation; ib, in-plane bending; ob, out-of-plane bending, t, torsion
[c]These modes involve minimal contribution from the NH group and can undergo a slight (~5–15 cm^{-1}) downshift upon amide NH deuteration

frequencies, as shown in Table 2. The amide I mode is by far the most useful absorbance band in structural characterization of proteins and peptides. A protein that contains various secondary structures generates an asymmetric, composite amide I band. The fractions of distinct secondary structures in the protein are identified by curve-fitting procedures on the amide I band, as described below. Briefly, the fraction of each secondary structure in the protein (or peptide) is determined as the fraction of respective amide I spectral component. Corrections should be made with respect to the extinction coefficients of various secondary structures, as summarized in Table 3.

The amide II mode occurs around 1,570–1,540 cm^{-1} and includes a significant contribution from the NH in-plane bending, along with CN stretching and other vibrations of the amide group, and hence is highly sensitive to the kinetics of amide HX (i.e., amide NH to ND conversion). The amide III mode occurs in the 1,300–1,200 cm^{-1} region as a result of NH and C=O in-plane bending vibrations and CC stretching vibration, and hence is sensitive to amide HX (1). Although amide III band exhibits sensitivity to the polypeptide chain secondary structure and has been used in protein and peptide structural studies (3), this mode is affected by side chains and hence is likely to vary depending on the protein's amino acid composition (1, 4). Amide IV to amide VII modes

Table 2
Characteristic amide I wavenumbers (*W*) of various secondary structures in H_2O and D_2O

Secondary structure	W_{H2O} (cm^{-1})	W_{D2O} (cm^{-1})
α-Helix	1,658–1,647	1,655–1,638
α_{II}-Helix[a]	1,666–1,658	1,658–1,652
α-Helical coiled coil[b]	1,640–1,630	1,640–1,630
3_{10}-Helix	1,665–1,655[c]	1,665–1,655[c]
3_1-Helix[d]	1,639	1,632
β-Helix[e]	1,640–1,630	~1,630
Parallel β-sheet	1,638–1,632	1,636–1,630
Antiparallel β-sheet	1,638–1,632 (strong) and 1,695–1,675 (weak)	1,636–1,630 (strong) and 1,680–1,670 (weak)
Intermolecular (aggregated) β-sheet	1,627–1,615[f]	1,625–1,613[f]
α-Pleated sheet[g]	1,653–1,650	1,653–1,650
β-Turns	1,685–1,655	1,675–1,640
γ-Turns	1,690–1,650	1,690–1,650
Irregular ("unordered") structure	1,660–1,652	1,648–1,640

[a]α_{II}-Helix is similar to the regular α-helix (α_I-helix) but has tilted amide plane, which weakens the intramolecular H-bonding, resulting in a stronger C=O bond and higher amide I frequency (98, 103)
[b]From refs. (104, 105)
[c]Observed and calculated amide I wavenumbers for 3_{10} helix were in 1,665–1,655 cm^{-1} region (1, 106), but several researchers reported lower wavenumbers in the 1,640–1,630 cm^{-1} region (107, 108)
[d]The 3_1-helix is an extended helical structure, found, for example, in polyglycine, forming hexagonal lattice stabilized by intermolecular H-bonding (1)
[e]The β-helix is a helical structure of variable geometry found in polypeptides with alternating L-, D-chirality of amino acids such as gramicidin A or poly(γ-benzyl-LD-glutamate) (109, 110)
[f]From refs. (111–114)
[g]The α-pleated sheet is an extended, pleated structure with C=O and NH groups at opposite sides of the chain, predicted by Pauling and Corey (115) and found in amyloid peptides (116, 117) as well as certain proteins such as the selectivity filter of K^+-channel. (The amide I frequency for the non-deuterated form was calculated by Wu et al. (118))

occur at lower frequencies (750–200 cm^{-1}) and are used in protein structural studies less frequently because of their low intensities and moderate sensitivity to protein structure (1). Some of them involve large contributions from the NH vibration and can be used to study the amide HX kinetics. For example, the amide V mode results from NH out-of-plane bending and CN torsion vibrations and

Table 3
The peak absorbance extinction coefficients (ε) and the integrated absorbance extinction coefficients (B) for amide I and amide II modes of proteins in H_2O at 25°C[a]

Amide mode (second. structure)	ε ($M^{-1}cm^{-1}$)	B ($M^{-1}cm^{-2}$)
Amide I (α-helix)	700 ± 100	(7.6 ± 1.1) × 10^4
Amide II (α-helix)	300 ± 50	(2.9 ± 0.6) × 10^4
Amide I (β-sheet)	975 ± 10[b] 180 ± 20[c]	(6.9 ± 0.8) × 10^4 [b] (0.5 ± 0.05) × 10^4 [c]
Amide II (β-sheet)	340 ± 10	(3.3 ± 0.3) × 10^4
Amide I (irregular)	330 ± 50	(4.7 ± 0.5) × 10^4
Amide II (irregular)	220 ± 50	(3.7 ± 0.8) × 10^4

[a]Adapted from ref. (99). Disproportional changes in ε and B indicate change in the band lineshape (the band can become higher and slimmer, or shorter and broader, without changes in the area). For α-helix in D_2O, $\varepsilon_{Amide\ I}$ decreases to 465 ± 20 M^{-1} cm^{-1}, while for β-sheet and irregular structures, $\varepsilon_{H2O} \approx \varepsilon_{D2O}$
[b]Major, low-frequency β-sheet component (1,638–1,632 cm^{-1})
[c]High-frequency β-sheet component (1,695–1,675 cm^{-1})

undergoes a strong downshift upon amide HX. Amide A and amide B modes are generated by Fermi resonances between amide II and NH stretching vibrations and are located around 3,300 and 3,100 cm^{-1}, respectively. They are exceptionally sensitive to protein amide HX kinetics and in a few cases have been used for protein secondary structure characterization (5, 6). Certain amino acid side chains absorb appreciably in amide I and amide II regions and should be taken into consideration during data analysis. The absorbance wavenumbers generated by certain functional groups of amino acid side chains and respective extinction coefficients are summarized in Table 4. More details on amide modes and other infrared spectroscopic features of proteins and peptides can be found elsewhere (1, 7).

FTIR of proteins and peptides is normally conducted on samples in buffers made using D_2O rather than H_2O because the H–O–H bending vibration of H_2O strongly absorbs around 1,645 cm^{-1} and obscures the most important conformation-sensitive amide I band of the protein or the peptide (8–10). In addition, the broad and intense H–O–H stretching bands between 3,500 and 3,200 cm^{-1} mask the amide A mode (Table 5). D_2O is transparent in these regions; it weakly absorbs in the amide II region (1,555 cm^{-1}), and HOD absorbs in the deuterated amide II region (1,450 cm^{-1}), which should be taken into consideration in amide II band analysis. While the molar extinction coefficients of H_2O or D_2O vibrational modes are approximately an order of

Table 4
FTIR wavenumbers [W (cm^{-1})] of various vibrational modes of certain amino acid side chains and terminal amino and carboxyl groups, the peak absorbance extinction coefficients [ε (M^{-1} cm^{-1})], and the integrated absorbance extinction coefficients [B (M^{-1} cm^{-2})] in H_2O and D_2O[a]

Amino acid	Mode[b]	W_{H2O}	ε_{H2O}	B_{H2O}	W_{D2O}	ε_{D2O}	B_{D2O}
Arginine	$CN_3H_5^+$ as	1,673	420	4.3×10^4	1,608	460	3.1×10^4
	$CN_3H_5^+$ ss	1,633	300	3.6×10^4	1,686	500	3.4×10^4
Asparagine	C=O s	1,678	310	2.7×10^4	1,648	570	5.2×10^4
	NH_2 d	1,622	160	2.5×10^4			
Aspartic acid	COO^- as	1,574	380	5.5×10^4	1,584	820	8.8×10^4
	COOH s	1,716	280	4.1×10^4	1,713	290	3.5×10^4
Glutamine	C=O s	1,670	360	3.1×10^4	1,635	550	5.8×10^4
	NH_2 d	1,610	220	3.5×10^4			
Glutamic acid	COO^- as	1,560	470	7.1×10^4	1,567	830	8.9×10^4
	COOH s	1,712	220	3.6×10^4	1,706	280	3.4×10^4
Histidine	Ring	1,596[c]	70	3.0×10^3	1,620[d]	6	2.5×10^2
					1,623[e]	16	8.0×10^2
					1,600[e]	35	1.5×10^3
Lysine	NH_3^+ ad	1,629	130	1.8×10^4			
	NH_3^+ sd	1,526	100	1.3×10^4			
Phenylalanine	Ring	1,494	80	2.0×10^3	1,607	10	5.0×10^2
					1,596	10	5.0×10^2
Tryptophan	Ring				1,545	10	5.0×10^2
Tyrosine	Ring	1,518[f]	430	1.0×10^4	1,615[f]	160	5.0×10^3
		1,602[g]	160	7.0×10^3	1,515[f]	500	1.1×10^4
		1,498[g]	700	2.5×10^4	1,603[g]	350	1.8×10^4
					1,500[g]	650	2.9×10^4
α-Amino group	NH_2 d	1,560	450	7.5×10^4			
	NH_3^+ ad	1,630	210	3.8×10^4			
	NH_3^+ sd	1,515	200	4.3×10^4			
α-Carboxyl group	COOH s	1,735	170	2.1×10^4	1,720	230	2.7×10^4
	COO^- as	1,598	240	3.5×10^4	1,594	830	8.4×10^4

[a]Adapted from refs. (119, 120)
[b]as = asymmetric stretching; ss = symmetric stretching, ad = asymmetric deformation, sd = symmetric deformation, d = deformation, s = stretching
[c]Imidazole absorbance parameters in H_2O did not change upon protonation (119)
[d]Non-protonated imidazole ring in D_2O produces one weak band
[e]Protonated imidazole ring in D_2O produces two bands
[f]The (−OH) form of the ring produces one narrow band in H_2O and two bands in D_2O
[g]Deprotonated ($-O^-$) ring produces two bands in both H_2O and D_2O

Table 5
FTIR vibrational wavenumbers (*W*) of H_2O, D_2O, and HOD; the peak absorbance extinction coefficients (ε); and the integrated absorbance extinction coefficients (*B*) at 25°C[a]

Vibrational mode[b]	*W* (cm^{-1})	ε (M^{-1} cm^{-1})	*B* (M^{-1} cm^{-2})
HOH as	3,490 ± 20	122 ± 20[c]	(28 ± 4) × 10^3 [c]
HOH ss	3,280 ± 20	106 ± 16 [c]	(25 ± 3) × 10^3 [c]
HOH a	2,125 ± 10	3.4 ± 0.4	(3 ± 0.3) × 10^2
HOH b	1,645 ± 4	20 ± 2	(1.6 ± 0.3) × 10^3
DOD as	2,540 ± 20	120 ± 20 [c]	(19 ± 2) × 10^3 [c]
DOD ss	3,450 ± 20	110 ± 12 [c]	(17 ± 2) × 10^3 [c]
DOD a	1,555 ± 20	1.9 ± 0.05	(1.2 ± 0.2) × 10^2
DOD b	1,215 ± 20	16 ± 1	(1 ± 0.1) × 10^3
HOD ss	3,380 ± 20	120 ± 20 [c]	(8 ± 1) × 10^3 [c]
HOD as	2,500 ± 20	108 ± 15[c]	(7 ± 1) × 10^3 [c]
HOD b	1,450 ± 20	18 ± 2	(1.6 ± 0.4) × 10^3

[a]Adapted from refs. (8–10)
[b]as = asymmetric stretching, ss = symmetric stretching, a = association, b = bending
[c]Asymmetric and symmetric stretching extinction coefficients apply to the whole molecule rather than a single OH or OD vibration

magnitude weaker than those of amide I or amide II bands (Tables 3 and 5), the large molar excess of the solvent (~55 M of solvent vs. $\leq 10^{-4}$ M of protein or peptide) makes the solvent contribution too large and hence strongly reduces the reliability of solvent subtraction procedures. Exposure of the peptide to D_2O initiates HX of the amide NH group. The vibrational frequency of a diatomic molecule can be approximately expressed as

$$\nu = \frac{1}{2\pi}\sqrt{k\left(\frac{1}{m_1}+\frac{1}{m_2}\right)}, \qquad (1)$$

where k is the spring constant, proportional to the chemical bond strength, and m_1 and m_2 are the atomic masses. Deuteration of the amide NH group results in a downshift of the amide A mode from ~3,300 cm^{-1} to 2,500–2,400 cm^{-1}; a shift of amide V and amide III modes from 725 cm^{-1} down to 510 cm^{-1}, and from ~1,250 to 960 cm^{-1}, respectively; a smaller but significant shifts of the amide II mode (~90 cm^{-1}); and a ~10 cm^{-1} downshift of the amide I mode. A set of FTIR spectra measured within several hours following exposure of the sample to D_2O allows determination of the

secondary structure of the protein/peptide as well as the amide HD kinetics. The latter reflects both the rigidity of protein's secondary structure and the degree of solvent accessibility. Deuteration of amide NH group occurs only when (a) it is exposed to D_2O and (b) is not H-bonded to C=O or other groups. Thus, a backbone NH group involved in a secondary structure such as α-helix of β-sheet can only undergo deuteration upon a transient breakage of the H-bond ("local breathing") provided it is exposed to the D_2O solvent. Since the breakage occurs less frequently in rigid secondary structures, a faster amide HX may reflect a more flexible structure, a higher degree of solvent accessibility, or a combination of the two. The information gained from amide HX measurements often is considered to reflect the protein's "dynamic structure" or the "structural dynamics," that is, the degree of molecular flexibility plus the tightness of the three-dimensional packing.

Analysis of the FTIR spectra of proteins or peptides usually provides global structural information, that is, the fractions of various secondary structures, without identification of their locations within the protein molecule. There are at least two procedures that can be used to locate the experimentally determined secondary structures along the polypeptide chain. First, application of a secondary structure prediction algorithm to the amino acid sequence identifies stretches that are most likely in α-helical, β-strand, turn, or irregular conformations. Internet-based secondary structure prediction programs are available, such as Psipred, provided by University College London Department of Computer Science (http://bioinf.cs.ucl.ac.uk/psipred/), or Jufo, provided by Professor Jens Meiler's lab of Vanderbilt University (http://www.meiler-lab.org/index.php/servers/show). If the predicted and experimental secondary structure contents are similar, then the FTIR-derived secondary structures can be assigned to the predicted regions. In the absence of consensus, site-specific structural information can be obtained by isotope labeling of desired regions of the protein or the peptide. This can be done by using synthetic, semi-synthetic, or metabolic methods, described in detail below. Labeling of single or multiple amino acids with isotopes such as ^{13}C results in a downshift of the vibrational frequency of the amino acid (s) containing the heavier atom, according to Eq. 1, and thus allows spectral resolution and site-specific structural characterization of the protein. Isotopic enrichment is also used to study protein–protein interactions. When one of the interacting proteins is ^{13}C-labeled and the other is not labeled, then the sample containing both proteins generates a split amide I band, the higher and lower frequency components corresponding to unlabeled and ^{13}C-labeled proteins. Curve-fitting of both components and comparison of the data with those obtained on each protein separately allows evaluation of the structural changes occurring in the two proteins upon interaction.

Membrane proteins have been studied by FTIR spectroscopy using both conventional, "direct transmission" technique and the ATR-FTIR technique (7, 11, 12). In the former case, the protein is either solubilized in a membrane-mimetic environment such as a detergent or reconstituted in lipid vesicles, followed by placing the sample between two IR windows and measurement of the spectra. For integral proteins or peptides, which are highly hydrophobic and therefore reside exclusively within the detergent or the membrane, this method is completely justified and provides valuable structural information. For peripheral proteins, which are water soluble yet bind to membranes when they are present, the direct transmission method may not be an optimal choice because a fraction of the protein may reside in the aqueous phase. The spectra will reflect the structures of both free and membrane-bound species, preventing an unambiguous determination of membrane-induced conformational effects.

ATR-FTIR spectroscopy provides several advantages in structural characterization of membrane proteins. High-quality spectra can be obtained on a single lipid bilayer containing the reconstituted protein, requiring only ~100 μg of lipid and several times lower amounts of protein. Stacked bilayers can be easily prepared on the internal reflection element (IRE), which significantly increases the signal intensity and, correspondingly, the signal-to-noise ratio, and prevents interactions of the membrane-incorporated protein with the solid substrate. A pair of ATR-FTIR spectra, measured at *p* and *s* polarizations of the incident light, allows evaluation of the secondary structure of the membrane-bound protein by curve-fitting of the amide I band, the orientation of the protein from the linear dichroic ratios, the amide HX kinetics from the time-dependent changes in the amide II band, the phase state of the lipid from the acyl chain methylene stretching frequencies, the lipid order parameter from the acyl chain dichroism, the hydration state of the membrane from the lipid carbonyl stretching frequency and lineshape, membrane binding affinity and stoichiometry of the protein, and more (7, 11–16). This method is particularly useful to study the mechanisms of interfacial enzymes, that is, the enzymes that bind to membranes, undergo activation, and acquire their substrate, such as lipid or fatty acid molecules, from the membrane (13, 16–18). Using segmentally ^{13}C-labeled PLA_2, the angular orientation of membrane-bound enzyme has been determined, which, in combination with fluorescence and modeling results, produced the mode of membrane binding of the protein at an atomic resolution (19).

Below, a more detailed description of FTIR and ATR-FTIR spectroscopy of proteins and peptides in lipid membranes is provided, including experimental and data analysis protocols. A number of examples are presented to demonstrate what these techniques can provide in terms of structural, and sometimes

functional, characterization of membrane proteins or peptides. As such, this article is a practical guide of FTIR and ATR-FTIR spectroscopy of membrane proteins and peptides rather than a review of literature.

2. Materials

2.1. Buffers

Buffers for FTIR experiments can be prepared using H_2O or D_2O. Since H_2O strongly absorbs in the 1,700–1,600 cm^{-1} region and thereby obscures the conformation-sensitive amide I band (Table 5), D_2O is the preferred solvent in FTIR spectroscopy of proteins or peptides. In certain cases, for example, when the amide II band is to be measured in an unperturbed state (i.e., without amide deuteration), measurements can be conducted in H_2O-based buffers, which are prepared by conventional methods. D_2O-based buffers can be prepared using a regular pH meter, provided certain precautions are exercised. A typical, simple buffer for protein or peptide FTIR studies is described below:

1. 100 mM NaCl, 20 mM Hepes, pH* 6.8.

Here, pH* 6.8 is the pH meter reading and corresponds to real deuterium ion concentration equivalent to pD = 7.2. The isotope effect results in 0.4 pH unit difference between pD and pH*: pD = pH* + 0.4 (20, 21). The procedures of buffer preparations are as follows:

1. Weigh the amounts of NaCl and Hepes required for a certain volume (e.g., 200 mL) of buffer and dissolve in ~150 mL of D_2O.
2. Calibrate the pH meter with standard buffers.
3. Rinse the electrode with D_2O to remove traces of H_2O, and immerse the electrode into the solution while stirring with a magnetic stir bar.
4. Titrate the solution with a NaOH solution of relatively high concentration (knowledge of the exact NaOH concentration is not necessary) until the desired pH meter reading (i.e., pH*) is reached. This should be 0.4 U below the pH of the medium to be imitated (see above). Other buffers, such as Tris or phosphate, can be used (Tris will be titrated with HCl or other acids). Ideally, NaOD and DCl should be used to minimize the presence of protons, and hence formation of H_2O, in the solution, but using NaOH or HCl has not led to significant problems.
5. Once the target pH* is reached, add D_2O to achieve the final volume of the buffer and store at 4°C.

2.2. Lipids

Lipids for preparation of artificial membranes, such as vesicles or supported bilayers, are available from various vendors. Using synthetic lipids may be preferred over the lipids isolated from biological tissues, such as bovine brain or liver, because these may contain trace contaminants of biological origin. When modeling a certain type of cellular membrane, such as endoplasmic reticulum, mitochondrion, or plasma membrane, it is advisable to use a mixture of lipids that mimic the respective membrane lipid composition, including both the headgroups and the degree of hydrocarbon chain unsaturation.

2.3. Proteins

Proteins are usually obtained by overexpression in prokaryotic or eukaryotic systems and purification using chromatographic methods. For structural studies, the purity of the sample is critical; hence care should be taken to reach a single spot in SDS gels upon staining with silver (22). Coomassie staining is less sensitive and may not detect relatively significant contaminations. Proteins uniformly labeled with certain isotopes, such as ^{13}C or ^{15}N or both, can be obtained by growing the plasmid-transfected cells in a minimal medium (e.g., M9) that contains 2.0–4.0 g/L of U-$^{13}C_6$-D-glucose and/or 5.0 g/L $^{15}NH_4Cl$ as single metabolic sources of carbon or nitrogen, respectively (23, 24). This will work with bacteria that can synthesize all 20 amino acids. When mammalian cells are used as an expression system, the medium should contain not only U-$^{13}C_6$-D-glucose or $^{15}NH_4Cl$ but also the isotope-labeled essential amino acids, which cannot be synthesized by mammalian cells. For example, the Bioexpress-6000 (Mammalian) medium from Cambridge Isotope Laboratories contains isotope-labeled Gln, His, Ile, Leu, Lys, Met, Thr, Val, Phe, and Trp.

In some cases, a certain amino acid in the protein can be labeled with a desired isotope by using an auxotroph, such as an *Escherichia coli* strain that is unable to make the amino acid (25, 26). The labeled amino acid should be present in the cell culture medium so the cells will incorporate it in all proteins during biosynthesis. Multiple *E. coli* strains that are auxotroph for any one of the 20 amino acids have been engineered by gene knockout methods (see http://cgsc.biology.yale.edu/Auxotrophs.php.) If the amino acid is present at multiple positions of the target protein, correspondingly multiple sites will be labeled, which may not be an optimal situation for gaining site-specific structural information. Insertion of an isotopically or otherwise modified amino acid into a desired site of a protein is more difficult. One of the widely used methods is the nonsense suppression protein engineering method (27–31). At the target site in the sequence of plasmid DNA, the codon is replaced with one of the three stop (nonsense) codons, such as TAG. A tRNA with a respectively modified anticodon loop (e.g., $tRNA_{CUA}$) that is complementary to the nonsense codon (in this

case, UAG in mRNA) is created by chemical or recombinant methods. The modified tRNA is then charged with an unnatural or labeled amino acid either chemically or enzymatically, using a mutated aminoacyl tRNA synthetase. Addition of the $tRNA_{CUA}$ loaded with the modified amino acid to the growth medium of cells transfected with the plasmid containing TAG at the target site will produce the protein with the modified amino acid at the desired site. TAG is not used by bacteria frequently as a stop codon, so $tRNA_{CUA}$ will interact only with the UAG codon in the mRNA generated by the expression plasmid. On the other hand, the premature termination of translation can be excluded by thermal inactivation or removal of the release factors specific to the utilized stop codon, using cell-free expression systems. Incorporation of more than one modified amino acid in a protein has been achieved by using codons containing three, four, or five nucleotides (32, 33).

Labeling just one residue in a protein with ^{13}C, or ^{13}C and ^{15}N, may not generate a strong enough signal to be distinguished from the amide I band generated by the unlabeled part of the protein. In addition, distinct amide I frequencies generated by each secondary structure are determined by vibrational coupling between neighboring amide units, implying that the FTIR signal from a lonesome ^{13}C-labeled (uniformly or carbonyl ^{13}C=O-labeled) amino acid cannot provide reliable information on the local secondary structure, even when it is spectrally resolved. These drawbacks can be remedied by labeling a whole segment of the protein rather than just one residue. Segmental labeling of proteins with stable isotopes for FTIR studies has been achieved by protein semisynthesis methods (19, 34). Isotope-edited FTIR is described in detail in Subheading 5 below.

2.4. Peptides

Peptides can be obtained by recombinant expression as proteins. However, numerous companies offer peptide synthesis services at an affordable price, which makes the custom order of synthetic peptides the preferred option of obtaining pure peptides of any sequence, containing 50 and more amino acid residues. The peptide sample often contains trifluoroacetic acid (TFA) that is being used for cleavage of the peptide from the solid phase support after synthesis and/or for purification by HPLC. TFA strongly absorbs in the amide I region, around 1,674 cm^{-1}; therefore it should be removed before analysis of the peptide by FTIR. This can be done easily by two or three cycles of dissolving the peptide in HCl (2–100 mM HCl has been used) or 0.1 % phosphoric acid solution followed by lyophilization, which results in replacement of TFA with chloride or phosphate anions as a counterion of cationic amino acid side chains (2, 35, 36). It is advisable to use pure H_2O for one or two additional cycles to remove the traces of the acid.

The synthetic method offers additional advantages. For example, isotopically labeled or unnatural amino acids can be easily

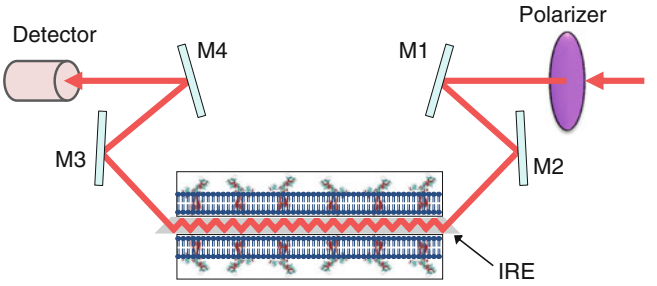

Fig. 2. A version of ATR-FTIR experimental setup for measurements of the spectra of a supported membrane with a reconstituted protein. The *gray trapezoid* is an internal reflection element (IRE), such as a germanium plate, which is covered with lipid bilayers at both surfaces (*blue*), containing the reconstituted integral protein shown in ribbon format. Mirrors M1 and M2 direct the incident light into the IRE, and mirrors M3 and M4 direct the light into the detector. Other details are described in the main text.

incorporated at any site in the peptide sequence during the synthesis (35–37). Also, any chemical groups, such as a C-terminal thioester for native chemical ligation experiments, can be added. As in the case of proteins, the amide I signal from one labeled residue may be lost in the large amide I band from the unlabeled part of the peptide and may not reflect the local secondary structure; hence labeling of a number of consecutive residues has been employed to gain site-specific structural information on peptides by FTIR (15, 35, 36, 38).

2.5. Direct Transmission FTIR Accessories

In addition to an FTIR spectrometer, certain accessories are used in a simple, direct transmission FTIR experiment. These include (1) a liquid sample holder, which usually slides vertically into the stand on the baseplate in the sample compartment of the spectrometer, (2) two infrared-transparent windows, such as CaF_2 or BaF_2 windows, (3) a spacer, that is, a thin ring that fits the circumference of the windows, made of Teflon or another inert and durable material (the reasonable thickness of the spacer is in the range 5–50 μm). If the spectrometer is using an MTC detector, approximately half a gallon of liquid nitrogen will be needed to cool it down.

2.6. ATR-FTIR Accessories

ATR-FTIR measurements require (1) an ATR system composed of four vertically mounted mirrors directing the incident light into the sample and then to the detector (Fig. 2); (2) a vertical stage that holds the ATR system and allows adjustment of the height of the mirrors to maximize the signal; (3) an internal reflection element (IRE) that is transparent to mid-infrared light and has a greater refractive index than the lipid–protein sample, such as germanium, zinc selenide, or thallium bromoiodide (a.k.a. KRS-5) (diamond meets all IRE requirements but is prohibitively expensive and hence nonpractical); (4) a demountable, perfusable sample cell composed of two halves designed to sandwich the IRE between them; (5) a

polarizer, such as aluminum wire grid deposited on KRS-5 substrate; and (6) an argon plasma cleaner to treat the IRE before use. The size of the IRE may be 5.0 × 2.0 × 0.1 cm^3, cut at 45° aperture angles at the 2.0 cm sides. If the substrate-supported membrane is to be prepared using a Langmuir–Blodgett method, a monolayer trough will be required.

3. Methods

3.1. Direct Transmission FTIR Measurements

3.1.1. Acquisition of Protein Spectra

As explained above, FTIR of proteins or peptides is conducted using D_2O-based buffers. The main reason for this is that D_2O is transparent in the amide I region, while H_2O strongly absorbs around 1,645 cm^{-1} (Table 5). Using D_2O has additional advantages. The α-helical and irregular structures absorb in overlapping regions in both H_2O and D_2O (Table 2). However, the unordered structure undergoes amide HX much faster (seconds) than the α-helix (minutes to hours) (14). Thus, a protein sample that is exposed to D_2O for about 0.5–1.0 h produces an amide I band where the irregular component is mostly exchanged while the α-helical component is still unexchanged, thus allowing for spectral resolution and estimation of the relative contents of both structures in the protein. Prolonged exposure to D_2O will result in exchange of all secondary structures, again preventing distinction between α-helix and irregular structure. (Note that absorbance bands of deuterated proteins or peptides are denoted amide I', amide II', etc.)

The best strategy is to measure the spectrum in an H_2O-based buffer and then prepare a sample in a D_2O-based buffer and record spectra over time, for 1–2 h or more. The spectrum measured in H_2O will provide the amide II band intensity, and those measured in D_2O will show a gradual decrease in the amide II band intensity in the 1,570–1,540 cm^{-1} region, reflecting the amide HX kinetics. At each time point, the extent of amide HX will be given by the relative amide II intensity, that is, the ratio of amide II band area measured at a given time divided by the area measured in H_2O, provided same protein concentrations and optical path-length are used in both cases. If this is not the case, the spectrum measured in H_2O should be normalized relative to an absorption band that is not exchangeable and hence should have the same intensity in all spectra, measured in H_2O and D_2O. This spectral feature should not overlap with solvent bands. An extrinsic compound with relatively high extinction coefficient can be used for such purpose. Finally, the amide I band of a protein in D_2O also undergoes spectral downshift due to amide HX and hence can be used to determine amide HX kinetics as well (12, 14).

For direct transmission FTIR experiments, it is convenient to have the protein or the peptide sample in lyophilized form:

1. Dissolve a certain amount of the lyophilized sample, typically 30–100 μg, in ~50 μL of a D_2O-based buffer and place on a CaF_2 or other window in a demountable liquid sample cell. The spacer should be placed on the window in advance.
2. Place the second window on top of the sample, which forms a thin layer between the two windows separated by the spacer.
3. Assemble the cell and mount in the sample cell holder in the spectrometer. These procedures should be done quickly to decrease the time lapse between the start of HX and first measurement.
4. It is customary to visually inspect the sample against light to see if voids ("air bubbles") are present. If large voids are present, which may result from greasy windows, for example, the window should be cleaned and a new sample should be prepared.
5. Start collection of spectra immediately after placing the sample in the spectrometer.
6. The lid of the sample compartment should be closed and the instrument continuously purged with dry air. Additional passage of the air through an air drying column, such as silica-gel column, results in very efficient removal of humidity and hence allows one to obtain "clean" spectra free of water vibrational modes in the amide I and amide A regions.
7. Record consecutive transmission spectra by collecting any number of scans per spectrum. A large number of scans, such as 500–1,000, will generate a better quality spectrum but will take a longer time, reducing the time resolution of amide HX kinetics. Around 10–50 scans may yield spectra of acceptable quality, especially when a high-sensitivity MCT detector is used. About 20 spectra collected within the first 2 h of amide deuteration (i.e., exposure of the sample to D_2O) will provide enough data for characterization of the structure and amide HX kinetics of the protein.
8. Following the collection of a set of sample transmission spectra, wash the cell and load with the blank buffer.
9. Measure spectra of the buffer, that is, the reference (or background) at same parameters as the sample.
10. In addition, two spectra of the "open beam" can be measured, corresponding to different times of purging with dry air after closing the lid of the sample compartment. Using an empty cell with the two windows separated by the spacer is not recommended because these measurements are usually affected by interference fringes. The two transmission spectra of the open

beam can be used to calculate an absorbance spectrum, using the first as "sample" and the second as "reference," to obtain a spectrum of atmospheric water vapor.

11. Each protein sample transmission spectrum can be paired with a buffer transmission spectrum to get an absorbance spectrum that is minimally affected by humidity.
12. If upward or downward spikes of water vapor absorbance are still present, they can be removed by spectral subtraction or addition of the water vapor spectrum. These procedures usually result in high-quality spectra that do not need any further smoothing unless needed for second derivative or other procedures.

3.1.2. Reconstitution of Proteins and Peptides in Lipid Vesicles

Procedures involved in preparation of membrane-bound protein samples depend on the nature of the protein. For peripheral proteins, which are water soluble but bind to membranes when they are present, the lipid vesicles can be prepared, followed by mixing with the protein solution. The extrusion method is an efficient and easy way of preparation of unilamellar vesicles of defined size:

1. If the lipid is provided in powder form, weigh a certain amount of lipid powder and dissolve in chloroform to obtain a stock lipid solution; a 10-mM concentration is customary. If chloroform does not dissolve the lipid, try a 2:1 (v:v) mixture of chloroform with methanol.
2. Transfer a desired amount of lipid solution into a small (e.g., 2–4 mL) glass vial and remove the solvent under a stream of nitrogen, followed by desiccation for ~3 h (desiccation for up to 12 h will not hurt).
3. Add a desired aqueous buffer to the dry lipid, followed by vortexing. This yields multilamellar vesicles (liposomes), unless the lipid has an intrinsic property of forming other, nonlamellar structures. For example, cardiolipin tends to form an inverted hexagonal structure, especially in the presence of calcium ions (39).
4. Extrude the liposome suspension through polycarbonate or other membranes with defined pore size, such as 100 nm or larger, using an extruder (40). About ten cycles of extrusion yield unilamellar vesicles with a homogeneous size distribution.
5. Prepare the protein solution in the same or similar buffer and mix with the vesicles. Avoid osmotic shock, that is, make sure the buffers used for preparation of the vesicles and the protein solution have similar osmolarities. This will result in binding of the protein to the external surface of the vesicles (17).

Alternatively, the vesicles can be prepared in the presence of the protein, resulting in binding of the protein to both external and

internal membrane surfaces. This latter option may not be an optimal choice, however, because extrusion may adversely affect the protein. If the spectra of a membrane-bound protein need to be measured, the lipid and protein concentrations should be chosen in a way that nearly all of the protein is bound to vesicles. This can be estimated using the protein-membrane binding constant and stoichiometry, measured separately (22, 40, 41). In the same time, the lipid/protein molar ratio should be kept within a reasonable range. In most cases, a considerable fraction of the protein may be free in solution rather than membrane bound, unless membrane binding is extremely strong. This implies that direct transmission FTIR is not the best choice for measuring the spectra of membrane-bound peripheral proteins; ATR-FTIR offers a number of advantages, as described below.

Reconstitution of integral proteins or peptides in vesicle membranes is relatively easy (14, 15):

1. Dissolve the peptide in an organic solvent, such as hexafluoroisopropanol, trifluoroethanol, or chloroform. Avoid using solvents that absorb in the amide I or amide II regions.
2. Mix the peptide solution with the solution of lipid in chloroform or chloroform/methanol (2:1, v/v) at a desired molar ratio.
3. Remove the solvent under a stream of nitrogen followed by desiccation.
4. Suspend the dry peptide/lipid sample in a buffer and extrude (see above).

This method works for most peptides. The hydrophobic nature of the peptide, which may correspond, for example, to the transmembrane stretch of an integral membrane protein, ensures its partitioning into the membrane. The organic solvents are likely to affect the peptide structure, but it may recover its membrane-bound structure following reconstitution.

Using organic solvents for membrane reconstitution of proteins may not always be advisable because they can denature the protein (42, 43). If the protein is overexpressed in a cell culture and purified, an appropriate detergent can be used as a component of the purification buffer, at a concentration two- to threefold above its critical micelle concentration (cmc). Detergents suitable for membrane protein reconstitution have been thoroughly studied (43, 44). The hydrophobic protein will partition into the detergent micelles, which can be isolated by size-exclusion or affinity chromatography or by density gradient centrifugation. The micelles then can be mixed with the preformed lipid vesicles, so the detergent concentration drops below its cmc, resulting in spontaneous partitioning of the protein into the vesicle membranes (14). Alternatively, the detergent-solubilized protein can be incubated with the

vesicles and SM-2 Bio-beads (Bio-Rad) for several hours. The high affinity of the Bio-beads for the detergent results in detergent partitioning into the Bio-beads and transfer of the protein into the vesicle membranes (45, 46). The vesicles, containing the reconstituted protein, then can be separated from the Bio-beads and used for FTIR measurements. One drawback of these procedures is that if an H_2O-based buffer is used, amide I spectra may be masked by the H_2O bending mode, and if a D_2O-based buffer is used, the protein will be extensively deuterated before the first spectrum is recorded, preventing measurements of amide HX kinetics. Again, ATR-FTIR may be considered a better choice for analysis of the structure and dynamics of membrane proteins (see below).

3.2. Direct Transmission FTIR Data Analysis

3.2.1. Protein Secondary Structure

The secondary structure of a protein or a peptide is usually evaluated by curve-fitting of the amide I absorbance band. The number and locations of amide I band components can be obtained from the second derivative spectra, the downward peaks of which indicate the amide I components. Often the inverted second derivatives are used, where the upward peaks point to the locations of the components (Fig. 3). Once the number of the amide I components and their spectral locations (the wavenumbers) are determined, a curve-fitting program such as GRAMS can be used to reproduce the actual amide I components. Gaussian or Lorentzian lineshapes, or a linear combination of the two, are being used. The curve-fitting procedure is considered satisfactory when (a) the deviation between peak wavenumbers of the components and those predicted by the second derivative does not exceed the nominal spectral resolution, for example, 2 cm^{-1}; (b) the sum of all components (the "curvefit") fits the actual amide I band; and (c) the widths of the components are within reasonable limits, for example, between 15 and 40 cm^{-1}. The components corresponding to the side chains, that is, those within 1,615–1,600 cm^{-1} (1,570–1,555 cm^{-1} for a ^{13}C-labeled protein), are subtracted, and the sum of the areas of all remaining components is used as the total amide I area (A_T). The components that correspond to α-helix, β-sheet, and irregular structure are identified following standard assignment procedures (Table 2). The antiparallel β-sheet has two components, a major, low-frequency component at 1,638–1,630 cm^{-1} and a high-frequency component at 1,695–1,675 cm^{-1}, and the integrated extinction coefficient of the latter constitutes ~7 % of the former (Tables 2 and 3). Therefore, the total β-sheet fraction can be determined by multiplying the fraction of the low-frequency β-sheet component area ($A_{\beta,low}$) by 1.07. The sum of the components between 1,700 and 1,660 cm^{-1} (1,655–1,615 cm^{-1} for a ^{13}C-labeled protein), minus 0.07 × $A_{\beta,low}$, then can be assigned to various types of turn structures. According to the Beer–Lambert law,

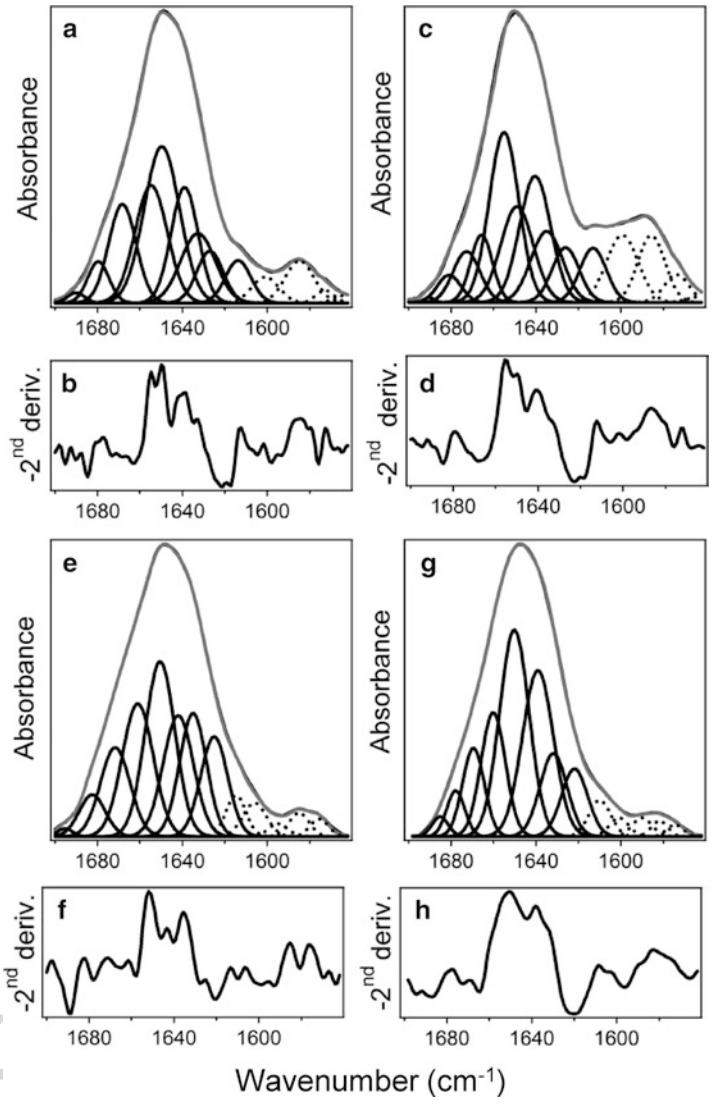

Fig. 3. Direct transmission (**a**, **c**) and ATR-FTIR (**e**, **g**) spectra of human group IIA PLA_2 (**a**, **e**) and its V3W mutant (**c**, **g**) either free in a buffer of 100 mM NaCl, 1 mM NaN_3, 1 mM EGTA, 50 mM Hepes in D_2O, pD 7.0 (**a**, **c**) or bound to a supported membrane composed of 70 % POPC and 30 % POPG, exposed to same buffer (**e**, **g**). ATR-FTIR spectra shown in panels **e**, **g** were obtained from the spectra measured at *p* and *s* polarizations of the infrared light as $A_p + 0.8A_s$. The components obtained by curve-fitting are shown for each spectrum; low-frequency components that are assigned to side chains are shown in *dotted lines*. The *gray lines* in (**a**), (**c**), (**e**), (**g**) are the sums of all components. Panels (**b**), (**d**), (**f**), (**h**) show the inverted second derivatives of spectra in panels (**a**), (**c**), (**e**), (**g**), respectively.

$$A_T = \sum l\varepsilon_i C_i, \qquad (2)$$

where l is the optical path-length and ε_i and C_i are the extinction coefficient and the concentration of the ith structural component,

Table 6
FTIR vibrational wavenumbers (*W*), bandwidths at half height (*BW*), relative amide I extinction coefficients (ε_{rel}), peak absorbance extinction coefficients (ε), and the integrated absorbance extinction coefficients (*B*) of various secondary structures of proteins in H_2O solutions at 20–25°C[a]

Secondary structure	*W* (cm^{-1})	*BW* (cm^{-1})	ε_{rel}	ε (M^{-1} cm^{-1})	*B* (M^{-1} cm^{-2})
Ordered α-helix	1,652	29.6	1.00	700 ± 100	$(7.6 \pm 1.1) \times 10^4$
Unordered helix + random str.	1,676	27.8	0.64	448 ± 64	$(4.9 \pm 0.7) \times 10^4$
	1,646	47.3	1.51	1,060 ± 150	$(11.5 \pm 1.7) \times 10^4$
	1,620	9.2	2.85	2,000 ± 300	$(21.7 \pm 3.1) \times 10^4$
β-Sheet	1,691	15.3	0.13	90 ± 15	$(1.0 \pm 0.1) \times 10^4$
	1,633	27.9	0.82	600 ± 80	$(6.2 \pm 0.9) \times 10^4$
Turns	1,720	46.7	0.17	120 ± 20	$(1.3 \pm 0.2) \times 10^4$
	1,668	21.8	0.20	140 ± 20	$(1.5 \pm 0.2) \times 10^4$
	1,629	9.1	0.26	180 ± 30	$(2.0 \pm 0.3) \times 10^4$
	1,613	23.3	0.10	70 ± 10	$(0.8 \pm 0.1) \times 10^4$

[a]Data in first four columns are from ref. (3). The extinction coefficients in columns 5 and 6 are calculated using the α-helical extinction coefficient reported by Venyaminov and Kalnin (99) and the relative extinction coefficients reported by Vedantham et al. (3)

side chains excluded. Eq. 2 yields the following expression for the concentration of *i*th secondary structure:

$$C_i = \frac{A_T - \sum_{j \neq i} l\varepsilon_j C_j}{l\varepsilon_i}. \quad (3)$$

The numerator in Eq. 3 is simply the area of the *i*th component, a_i; therefore, it can be rewritten as follows:

$$C_i = \frac{a_i}{l\varepsilon_i}. \quad (4)$$

The fraction of the *i*th secondary structure in the protein is

$$f_i = \frac{C_i}{C}, \quad (5)$$

where C is the total concentration of all secondary structural elements and is given as follows:

$$C = \sum \frac{a_i}{l\varepsilon_i}. \quad (6)$$

In Eq. 6, the summation is over all secondary structures. This approach requires the amide I areas and the extinction coefficients of all secondary structures (Tables 3 and 6). In some cases, the protein secondary structure can be presented as α-helix, β-sheet, irregular structure, and "other," primarily including turns and

other structures, or α-helix, β-sheet, irregular structure, turns, and "other." The problem here is that the extinction coefficient for the "other" structure is not known, but an extinction coefficient, which is the average of those of known structures, may be an acceptable approximation. If the α-helix, β-sheet, irregular structure (ρ), and "other" approach is adopted, then Eq. 6 can be rewritten as follows:

$$C = \frac{a_\alpha}{l\varepsilon_\alpha} + \frac{a_\beta}{l\varepsilon_\beta} + \frac{a_\rho}{l\varepsilon_\rho} + \frac{a_{other}}{l\varepsilon_{other}} \tag{7}$$

If the turn structures are included along with its extinction coefficients, then an additional term for the turns should be added. Equations 4, 5, and 7 yield

$$f_i = \frac{a_i}{\varepsilon_i\left(\frac{a_\alpha}{\varepsilon_\alpha} + \frac{a_\beta}{\varepsilon_\beta} + \frac{a_\rho}{\varepsilon_\rho} + \frac{a_{other}}{\varepsilon_{other}}\right)} \tag{8}$$

In case of spectra of two proteins combined in one sample, one unlabeled (i.e., ^{12}C) and other ^{13}C-labeled, the amide I components belonging to each protein should be identified keeping in mind that ^{13}C-labeling causes a 40–50 cm^{-1} spectral downshift. Together with respective extinction coefficients, eight fractions are found: $f_{\alpha,12C}$, $f_{\beta,12C}$, $f_{\rho,12C}$, $f_{other,12C}$, $f_{\alpha,13C}$, $f_{\beta,13C}$, $f_{\rho,13C}$, and $f_{other,13C}$ using Eq. 8 and are corrected as follows. Each of the eight fractions is multiplied by the total number of amino acid residues in two proteins and then divided by the number of amino acid residues in the respective (i.e., ^{12}C or ^{13}C) protein to determine the protein secondary structure.

Figure 3 shows an example of amide I band curve-fitting for human group IIA PLA_2 and its V3W mutant free in solution and bound to supported bilayers, using the second derivatives. Amide I components at 1,655 and 1,649 cm^{-1}, which are present in the spectra of both proteins in solution, have been assigned to non-exchanged and deuterated α-helix. These components constitute 19 and 28 % for the wild-type PLA_2 and 26 and 16 % for the mutant, indicating a faster amide HX in the former case. Upon membrane binding, the 1,655 cm^{-1} component shifts to 1,661 cm^{-1} and reduces in intensity in both cases, indicating formation of a more flexible α-helical structure. Weaker helical H-bonding corresponds to a stronger main chain C=O bond and a higher amide I frequency (see Eq. 1). Thus, FTIR provides information on protein secondary structure and the quality of helices, such as their relative rigidity. Formation of more flexible helices in group IIA PLA_2 is confirmed by amide HX data described below.

3.2.2. Amide HX Kinetics

The kinetics of amide HX is most frequently analyzed based on the time-dependent decrease in the amide II band intensity upon exposure to D_2O. In general, every single amino acid in a protein can undergo HX at a distinct rate depending on H-bonding, local

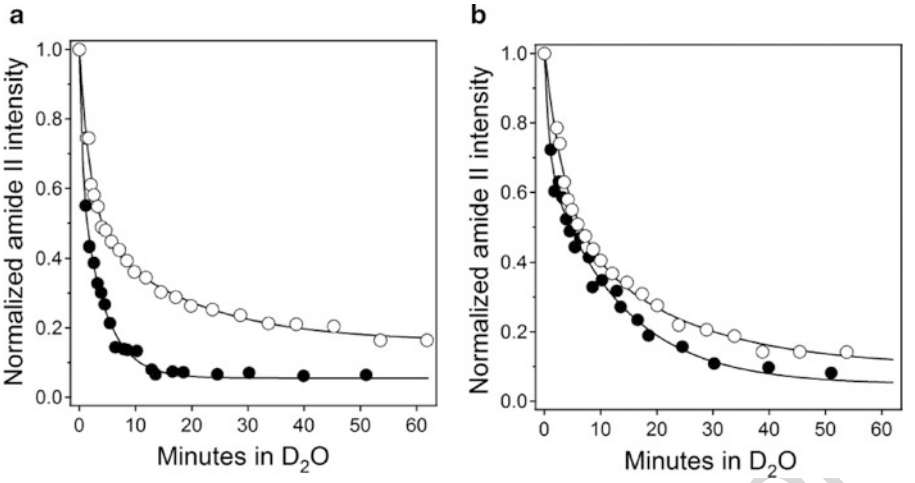

Fig. 4. Kinetics of amide HX for free (*open circles*) and membrane-bound (*closed circles*) human group IIA PLA_2 (**a**) and the V3W mutant (**b**), measured by polarized ATR-FTIR. The supported membrane was composed of 70 % POPC and 30 % POPG, and the buffer was 100 mM NaCl, 1 mM NaN_3, 1 mM EGTA, 50 mM HEPES (pH 7.0) in H_2O (at time 0) or D_2O (at time >0). The *solid lines* were calculated through Eq. 9, using the parameters summarized in Table 7.

mobility, structure, and steric protection from solvent. However, individual HX rate constants for each amino acid residue cannot be determined by conventional FTIR spectroscopy. Considering two to four populations, each characterized with a certain HX rate constant, usually allows a reasonable description of the overall HX kinetics of a protein. It is considered that each main chain amide group can be either in H form (non-exchanged) or D form (deuterated). The time dependence of the fraction of non-exchanged residues, [H/(H + D)], can be given as

$$\left[\frac{H}{H+D}\right]_t = \frac{A_{amideII,t}}{A_{amideII,0}} = a_0 + a_1 e^{-k_1 t} + a_2 e^{-k_2 t}, \qquad (9)$$

where $A_{\mathrm{amideII},0}$ and $A_{\mathrm{amideII},t}$ are the amide II band areas of the protein in H_2O and at time t of exposure to D_2O, respectively; a_0, a_1, and a_2 are the fractions of exchange-resistant, slow exchanging, and fast exchanging residues, respectively; and k_1 and k_2 are the exchange rate constants of the latter two populations. Since the protein can undergo adsorption to or desorption from the membrane during the measurements, it is advisable to use the ratio of the amide II area divided by the amide I area instead of just A_{amideII}, especially when analyzing ATR-FTIR data. Amide HX kinetics of PLA_2 free in solution and bound to supported membranes has been characterized using this approach (Fig. 4, Table 7). The data of Fig. 4 and the quantitative parameters of HX presented in Table 7 clearly indicate a more efficient HX of the protein upon membrane binding. This cannot be interpreted in terms of solvent protection upon membrane binding since it would have an opposite effect.

t.1 **Table 7**
Characterization of the amide HX kinetics of human group IIA PLA_2 and its V3W mutant free in solution or bound to a supported membrane composed of 70 % POPC and 30 % POPG, at 20°C[a]

t.2		Wild-type PLA_2		V3W mutant of PLA_2	
t.3		Free	Membrane-bound	Free	Membrane-bound
t.4	a_0	0.16	0.06	0.10	0.05
t.5	a_1	0.35	0.59	0.46	0.64
t.6	a_2	0.49	0.35	0.44	0.31
t.7	k_1 (min^{-1})	0.057	0.24	0.051	0.083
t.8	k_2 (min^{-1})	0.51	2.03	0.29	1.20

t.9 [a]Data from ref. (22). The data are described in Fig. 4

Instead, membrane binding renders the protein structure more flexible, resulting in an increased rate of HX, which is consistent with the data of amide I band curve-fitting described above.

In cases when amide II band intensity decreases very rapidly, spectral shifts in the amide I region can be used to evaluate the amide HX kinetics (12, 14). The amide I spectrum of the membrane-bound protein measured in an H_2O-based buffer is subtracted from a series of spectra measured at various times of exposure to D_2O. If a spectrum in H_2O cannot be measured, a spectrum of a sample that is exposed to D_2O for a very short time, for example, ~1–2 min, can be used. Since upon deuteration the amide I band undergoes a spectral downshift, the difference spectra will contain negative and positive components. All amide I areas can be normalized before subtraction. If the sum of the absolute values of all components of the difference spectra at time t of exposure to D_2O is ΔA_t, then the kinetics of the HX can be described by

$$1 - \frac{\Delta A_t}{r} = \sum_{i=0}^{m} a_i e^{-k_i t}. \qquad (10)$$

In Eq. 10, r is a proportionality coefficient relating spectral changes in the amide I and amide II regions:

$$r = \frac{\Delta A_t}{1 - \left(A_{amideII,t}/A_{amideII,0}\right)}.$$

and can be determined by measuring ΔA_t for the amide I band and $A_{\mathrm{amideII},t}/A_{\mathrm{amideII},0}$ at initial times of deuteration when the amide II band still can be measured reliably. Given the fact that FTIR does

not allow determination of a large number of individual amino acid HX kinetics, using $m = 2$–3, that is, considering an exchange-resistant population and 2 or 3 populations that undergo HX with similar kinetics, is considered a reasonable approach. Amide HX kinetics of SKC1 K^+ channel reconstituted in lipid membranes has been evaluated using both methods, that is, changes in the amide II region (Eq. 9) and amide I region (Eq. 10) and yielded consistent results (14). Approximately 80 % of all amino acid residues of the channel were able to undergo amide HX within ~3 h, consistent with a model of the channel containing water-filled vestibules.

3.3. ATR-FTIR Measurements

3.3.1. ATR-FTIR Sample Preparation and Measurements

ATR-FTIR experiments of membrane proteins have been conducted using a single lipid monolayer, a bilayer, or a multilayer (7, 11, 12, 46–49). Axelsen and coworkers used a germanium IRE rendered hydrophobic by treating it with octadecyltrichlorosilane (49–51). Positioning of the IRE horizontally against a lipid monolayer at the air–water interface, with the protein adsorbed to the lipid from the aqueous phase, allowed recording of polarized ATR-FTIR spectra.

A lipid bilayer supported on the IRE surface can be prepared using at least two methods. In both cases, the IRE, such as a germanium plate, should be thoroughly cleaned with organic solvent(s) such as a chloroform/methanol (2:1, v/v) mixture and processed with an argon plasma cleaned for about 10 min. The "monolayer fusion" method involves the following steps:

1. Deposit a lipid monolayer at both surfaces of the IRE, using a Langmuir–Blodgett trough.
2. Assemble the IRE in the ATR flow-through cell and inject a lipid vesicle suspension in an H_2O-based buffer, with lipid concentration between 1 and 10 mM. The lipid polar headgroups adsorb to the IRE surface, and the hydrocarbon chains are facing air, so the monolayer is stable for many hours. Using phosphatidylcholine for monolayer deposition works very well; acidic lipids do not adsorb to germanium efficiently probably due to electrostatic effects. Upon injection of the vesicles, they spread on the hydrophobic monolayer surface, resulting in formation of a supported bilayer. This process is driven by hydrophobic contacts between the vesicles and the monolayer as well as the curvature strain in the vesicle membrane (lipids such as phosphatidylcholine tend to form lamellar rather than curved structures). Therefore, highly curved vesicles, for example, those obtained by sonication, undergo spreading more readily. However, extruded vesicles of 100 nm diameter will work as well.
3. Allow the system to equilibrate for ~1–2 h.

4. Flush the cell with the buffer to remove excess lipid. If the vesicles are prepared in the absence of any peptides or proteins, the resulting membrane is a pure lipid bilayer that can be used to examine the lipid order, membrane phase state, etc. (12, 13, 16).

In the second method, the sonicated vesicles are prepared using at least 20–30 mol % of an acidic lipid, in a buffer containing ~5 mM $CaCl_2$ and directly injected into the ATR cell containing the IRE. Supported bilayers are formed spontaneously, probably stabilized by Ca^{2+} ionic bridges between the acidic lipids and the plate. In experiments with peripheral proteins, the protein solution can be injected into the ATR cell, followed by its adsorption to the supported membrane. The kinetics of membrane binding of the protein can be determined from the time-dependent increase in the amide I band intensity (13, 18). If an H_2O-based buffer is used, the amide II band can be monitored instead of amide I. Once the protein binding to the membrane stabilizes, the ATR cell is flushed with a D_2O-based buffer and polarized ATR-FTIR spectra are collected to determine the protein secondary structure and orientation. For example, consecutive pairs of *p* and *s* polarized spectra can be collected for 1–2 h, which can be used to determine the protein's secondary structure, the kinetics of amide HX, and the orientation with respect to the membrane (see below).

In experiments with integral proteins, the protein is reconstituted in vesicles, as described above, and after spreading of the vesicles on the lipid monolayer or directly on the IRE, appears in the supported bilayer. Other procedures are similar to those used with peripheral proteins.

The samples for ATR-FTIR experiments can be prepared using lipid–protein or lipid–peptide multilayers rather than a single bilayer, as described (48, 52, 53). The vesicles with the reconstituted protein are prepared in an H_2O-based buffer, at a high lipid and protein concentration, evenly spread on one surface of the IRE and dried under nitrogen and under vacuum. These "dry" samples then can be used directly for collection of ATR-FTIR spectra or can be hydrated by exposing to a D_2O-saturated atmosphere or to a D_2O-based buffer. The final sample is expected to be a multilamellar structure, that is, stacked bilayers containing the incorporated protein, more than 1 μm thick. While both lipids and proteins keep a nominal amount of bound water that cannot be removed by desiccation, the hydrated samples are considered more biologically relevant. In case of peptides, the solutions of the lipid and the peptide can be combined at a desired molar ratio and spread at one surface of the IRE followed by removal of the solvent. The lipid–peptide film then can be humidified by a D_2O-saturated atmosphere or by a bulk D_2O-based buffer.

The first exposure of the sample to D_2O is the time of initiation of amide HX. Consecutive spectra measured at *p* and

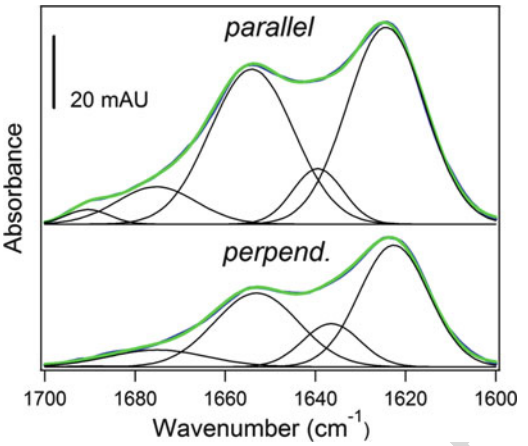

AU1

Fig. 5. ATR-FTIR spectra of a peptide derived from Bax protein in a supported POPC/POPG (7:3) multilayer at parallel and perpendicular polarizations, as indicated. The sample was exposed to a buffer of 150 mM NaCl, 10 mM Hepes in D_2O, pH* 6.8. The curvefit, that is, the sum of all amide I components shown under each spectrum, is in good fit with the measured spectrum. Major components at 1,655 cm^{-1} and 1,628 cm^{-1} indicate an α/β secondary structure.

s polarizations following exposure to D_2O are used to determine the protein's or peptide's secondary structure, orientation, and HX kinetics. Since most FTIR spectrometers are single beam instruments, reference spectra should be measured separately using a bare germanium plate or a sample prepared using plane lipid without any peptide or protein. Absorbance spectra at each polarization are obtained using the sample and reference transmission spectra at same polarization. Atmospheric water humidity spectra can be measured at both polarizations by collecting spectra at various times of purging with dry air, using a bare germanium plate. These water vapor spectra can be subtracted from sample absorbance spectra to clear the spectra from noise generated by residual humidity, when necessary. A pair of polarized ATR-FTIR spectra of a peptide in a 1.6 μm thick POPC/POPG multilayer is shown in Fig. 5, and the determination of the peptide's secondary structure and orientation based on the curve-fitted *p* and *s* polarized spectra is described in the next section.

3.3.2. ATR-FTIR Data Analysis

Polarized ATR-FTIR spectra can be used to evaluate the orientational order parameters of the lipid and the membrane-bound peptide or protein molecules, protein's and peptide's secondary structure, kinetics of amide HX, and more. The molecular order parameter can be determined from polarized ATR-FTIR experiments as (7, 47, 48, 54)

$$S = \frac{2B}{(3\langle\cos^2\alpha\rangle - 1)(B - 3E_z^2)}, \qquad (11)$$

where $B = E_x^2 - R^{ATR}E_y^2 + E_z^2$, E_x, E_y, and E_z are the electric vector components of the evanescent wave at the surface of IRE normalized relative to the incident light amplitude; α is the angle between the transition dipole moment and the molecular axis; R^{ATR} is the ATR dichroic ratio: $R^{\mathrm{ATR}} = A_p/A_s$, where A_p and A_s are the absorbance intensities at the peak of a band or integrated over the whole band for *p* and *s* polarizations of the infrared light, that is, parallel and perpendicular to the incidence plane, respectively; and the angular brackets indicate the average value. For the amide I (amide II) band, $\alpha = 38$–$40°$ (70–73°) for α-helix and ~90° (~0°) for β-strand (54–56); the latter only applies to the low-frequency β component at ~1,638–1,630 cm^{-1}. For methylene stretching vibrations of lipid hydrocarbon chains in all-trans conformation, $\alpha = 90°$. Two cases are considered, that is, a thin film sample, much thinner than the decay length of the evanescent wave, d_p, and a thick film sample, much thicker than d_p (in the amide I region, for a germanium-water system and a 45° incidence angle, $d_p \approx 320$ nm). For the thin film (57),

$$E_x = \frac{2\cos\gamma\sqrt{\sin^2\gamma - n_{31}^2}}{C}, \tag{12a}$$

$$E_y = \frac{2\cos\gamma}{\sqrt{1 - n_{31}^2}}, \tag{12b}$$

$$E_z = \frac{n_{32}^2 \sin 2\gamma}{C}, \tag{12c}$$

where γ is the incidence angle, $C = \sqrt{[(1 + n_{31}^2)\sin^2\gamma - n_{31}^2](1 - n_{31}^2)}$, and $n_{ij} \equiv n_i/n_j$, n_1, n_2, and n_3 are the refractive indices of IRE ($n_1 = 4$ for germanium), the thin layer of the sample ($n_2 \approx 1.43$ for a lipid layer), and the medium above the sample ($n_3 = 1$ for air and ~1.33 for water). If $\gamma = 45°$, then for a thin sample under air, $E_x = 1.411$, $E_y = 1.461$, and $E_z = 0.738$, and for a thin sample under water $E_x = 1.40$, $E_y = 1.51$, and $E_z = 1.375$. It is assumed that the sample is so thin that the evanescent field can be considered constant inside the sample. For a thick film, the evanescent wave does not exit the sample so only two phases are considered, the IRE and the sample. In this case, both n_2 and n_3 apply to the thick sample and $n_{32} = 1$, resulting in $E_z = 1.621$ (E_x and E_y stay the same). The average angle θ between the membrane normal and the molecular axis can be found from the relationship

$$S = \frac{1}{2}\left(3\langle\cos^2\theta\rangle - 1\right). \tag{13}$$

This theory can be applied to molecules that have a symmetry axis, such as lipid acyl chains in all-trans configuration or an α-helix.

In cases when a protein or a peptide contain a single α-helix, curve-fitting can be performed on amide I spectra measured at *p* and *s* polarizations, as shown in Fig. 5. The α-helical dichroic ratio, that is, the ratio of the areas of α-helical components at 1,655 cm^{-1} at *p* and *s* polarizations, then can be used to determine the helical orientation. Evaluation of the orientation of relatively large membrane-bound proteins, which may contain a variety of differently oriented helices and strands, is not easy. One way this can be achieved is isotope labeling of certain helices within the protein; combination of orientations of more than one helix allows positioning of the protein relative to the membrane (19). These procedures are described below.

Determination of the β-strand orientation is more complex. When the strands are arranged in a structure that is characterized by a central rotational axis, such as a β-barrel, the following holds (58):

$$\frac{1}{2}\left(3\langle\cos^2\delta\rangle - 1\right) = \frac{2B}{(3\langle\cos^2\chi\rangle - 1)\left(B - 3E_z^2\right)}, \qquad (14)$$

where δ is the angle of the transition dipole moment of β-strands with respect to the barrel axis and χ describes the orientation of barrel axis with respect to the membrane normal. For β-strands, the transition dipole moments of amide I and amide II modes are oriented perpendicular and along the strand axis, respectively (58). Therefore,

$$\delta_I = \frac{\pi}{2} - \beta \qquad (15a)$$

and

$$\delta_{II} = \beta \qquad (15b)$$

where subscripts I and II indicate amide I and amide II bands, respectively, and β is the angle between strand axes relative to the central axis of the barrel. Substitution of (15a) and (15b) into Eq. 14 yields two equations that can be solved together, using the experimentally determined dichroic ratios for amide I and amide II bands, to evaluate the angles χ and β.

In polarized ATR-FTIR spectra of a membrane-bound protein, the absorbance intensity of each structural element is determined by its spatial orientation among other things. Therefore, protein's secondary structure cannot be determined using a spectrum obtained at a certain polarization. ATR-FTIR spectra measured at *p* and *s* polarizations are used to generate a "polarization-independent" spectrum: $A = A_p + GA_s$, where the scaling factor G is given as (59)

$$G = \frac{2E_z^2 - E_x^2}{E_y^2} \qquad (16)$$

Using the values of E_x, E_y, and E_z shown above, we obtain $G = 0.80$ in case of a thin film between germanium plate and an aqueous medium and $G = 1.44$ for a thick film deposited on germanium. Once a corrected amide I spectrum is obtained, the curve-fitting can be performed and protein's secondary structure determined following the procedures described above. Curve-fitted *p* and *s* polarized amide I bands can also be used to obtain fractions of various secondary structures (59):

$$f_i = \frac{A_{p,i} + GA_{s,i}}{\sum \left(A_{p,i} + GA_{s,i}\right)}. \quad (17)$$

Application of both approaches to the polarized ATR-FTIR spectra of a membrane-reconstituted proteins or peptides yields similar results. For example, data shown in Fig. 5 indicate the following secondary structure for the membrane-bound peptide: $f_\alpha = 0.39$, $f_\beta = 0.40$, $f_t = 0.11$, and $f_\rho = 0.10$.

3.4. Isotope-Edited FTIR

3.4.1. Site-Directed Isotope Labeling

Since the conformation-sensitive amide I mode is generated primarily by the main chain C=O stretching vibration, site-directed labeling with ^{13}C or $^{13}C{=}^{18}O$ offers an opportunity to gain local structural information on peptides and proteins (2, 15, 35, 36, 60–64). The fact that through bond and through space vibrational couplings between interacting peptide group oscillators significantly contribute to the amide I frequencies should be given special consideration in interpretation of the signal generated by the labeled sites (2, 36, 63). Sensitivity of these couplings to the geometric arrangements of the oscillators renders the amide I frequencies dependent not only on distinct secondary structures but also on the distribution (e.g., consecutive vs. interrupted) of the isotope-labeled amide units (65). Introduction of one or two $^{13}C{=}O$ labels in a 14-residue β-sheet peptide resulted in a shift of the main amide I component from 1,628 cm^{-1} down to 1,611–1,606 cm^{-1} (2). The relative intensity of the downshifted component was significantly larger than the proportion of ^{13}C-labeled units, and this effect became more pronounced when the two ^{13}C labels were intervened by a single ^{12}C as compared to two adjacent ^{13}C labels. These anomalous intensity patterns were explained by a semiempirical treatment of vibrational couplings, including through covalent bonding, through H-bonding, and through space transition dipole couplings between ^{13}C and ^{12}C peptide units (2). Similar analysis on membrane-bound β-sheet peptides was performed by polarized ATR-FTIR, indicating that anomalously high intensities and frequencies of ^{13}C-generated amide I components can be explained by inter- and intra-strand couplings between ^{13}C and ^{12}C amide oscillators (63). The degree of spectral downshift and the relative intensity of the ^{13}C-labeled

amide mode were correlated with the type of β-sheet (parallel vs. antiparallel) and the number of strands in the sheet (2, 36, 63).

In contrast to peptides in β-sheet structure, the ^{13}C-labeled amide units in α-helical peptides appear to behave like isolated oscillators (2). Indeed, published data indicate that the vibrational coupling between amide units (peptide groups) containing ^{13}C-labeled and unlabeled (^{12}C) carbonyls depends on the secondary structure; ^{13}C–^{12}C coupling occurs readily in a β-sheet structure but not in an α-helical structure (36, 62, 63). While a single ^{13}C-labeled residue can provide local structural characterization of a peptide in β-sheet conformation (36, 62, 63), identification of a local α-helical structure requires at least three consecutive ^{13}C-labeled amide units, which will provide a directly connected pair of coupled ^{13}C oscillators that will generate the diagnostic vibrational frequency and intensity (15, 35, 36, 65). FTIR studies on helical peptides containing three or four consecutively ^{13}C=O-labeled residues revealed site-specific structural features, such as a higher thermal stability of the central region of an α-helix and relative conformational dynamics of C- vs. N-termini of peptides (35, 38).

Phospholamban transmembrane domain labeled with ^{13}C at one or two amino acids and reconstituted in supported lipid membranes was analyzed by polarized ATR-FTIR to gain insight into the local secondary structure and orientation (66). Such labeling resulted in ~45 cm^{-1} downshift in the amide I α-helical frequency from 1,658 to 1,614–1,612 cm^{-1}, as expected for decoupled oscillators, but the fact of decoupling raises questions about the meaning of the amide I mode of an isolated oscillator in terms of protein conformation or orientation. ATR-FTIR studies on glycophorin A transmembrane domain, ^{13}C-labeled at two or three consecutive sites, provided local structural and orientational information (67). The issue of helix or strand orientation determination by isotope-edited polarized ATR-FTIR was treated by Marsh (68). For a single site labeled peptide, linear dichroisms of more than one amide modes, such as amide I, II, and A, are required for helical orientation determination. For determination of the orientation of a β-sheet relative to the membrane plus the orientation of strands relative to the sheet, six dichroic ratios are required, which can be obtained from three different amide modes of two isotopically labeled residues.

Better amide I spectral resolution has been achieved by site-specific amino acid labeling with $^{13}C = {}^{18}O$ (69). $^{13}C = {}^{18}O$ labeled amino acids can be created by incubating the commercially available carbonyl ^{13}C-labeled amino acid in $H_2{}^{18}O$/dioxane (1:1 or 3:1, v/v) at 100°C at pH 1.0 for 1 h, followed by incorporation in the peptide sequence by chemical synthesis (69, 70). Care should be taken to avoid side chain modification of pH-sensitive amino acids. Labeling of the transmembrane domain of phospholamban with $^{13}C = {}^{18}O$ at either one of two centrally located adjacent

residues resulted in a significant downshift of the amide I signal from 1,657 to 1,590 cm^{-1}, allowing determination of the local transmembrane orientation by polarized ATR-FTIR (69). Transmembrane orientations and helix packing details on ErbB-2 and other integral membrane proteins were deduced from ATR-FTIR experiments on $^{13}C = {}^{18}O$ labeled peptides (53, 70, 71). Similar isotope editing strategies provided site-specific information on protein thermal stability and folding dynamics (72, 73), mechanisms of peptide aggregation (37, 74), and structural details of amyloid formation (75–77). Some of these studies used two-dimensional infrared spectroscopy (74–77), which is out of the scope of this text and has been reviewed elsewhere (78).

3.4.2. Structural Effects in Protein–Protein Interactions

Isotope-edited FTIR was used to gain insight into conformational changes in proteins upon their interactions. Uniform ^{13}C- or $^{13}C/^{15}N$-labeling of one of the two interacting proteins results in spectral resolution of their amide I bands and hence allows identification of conformational changes in both proteins (79–81). This strategy was utilized to detect structural changes in calmodulin and target peptides upon their interaction (80), as well as the structural effects involved in the chaperon-like activity of α-crystallin (81). Polarized ATR-FTIR studies on ^{13}C-labeled phospholamban and unlabeled sarcoplasmic reticulum Ca^{2+}-ATPase co-reconstituted in supported lipid bilayers identified that the inhibitory effect of phospholamban involved stabilization of α-helices of the Ca^{2+}-ATPase (46). More information on the analysis of protein–protein interactions by isotope-edited FTIR is provided elsewhere (82).

3.4.3. Segmental Isotope Labeling and Protein-Membrane Interactions

Labeling of a selected segment of proteins with ^{13}C can provide local conformational information. Moreover, for membrane proteins this strategy can provide the orientation of the membrane-bound protein. Using peptide ligation techniques (83–86), a semi-synthetic human pancreatic PLA_2 was engineered where the N-terminal helix was unlabeled, whereas the rest of the protein was uniformly ^{13}C-labeled (19). The procedure is schematically described in Fig. 6 and involved the following steps:

1. A peptide corresponding to the N-terminal α-helix of PLA_2 and containing a C-terminally added thioester group (Ala^1-Lys^{10}-$COSCH_2COOH$) was obtained by chemical synthesis.
2. A fragment of the protein starting with Cys^{11} was expressed in *E. coli* in a minimal medium containing 0.2 % uniformly ^{13}C-labeled D-glucose as a sole metabolic source of carbon.
3. The ^{13}C-labeled fragment Cys^{11}–Ser^{126} was reacted with a C-terminally thioesterified peptide in a buffer containing 6 M guanidinum-HCl, 100 mM Na-phosphate, 5 % β-mercaptoethanol, 1 mM EDTA, 4 % thiophenol, and 4 % benzyl mercaptan, pH 7.4. The concentrations of the C-terminal

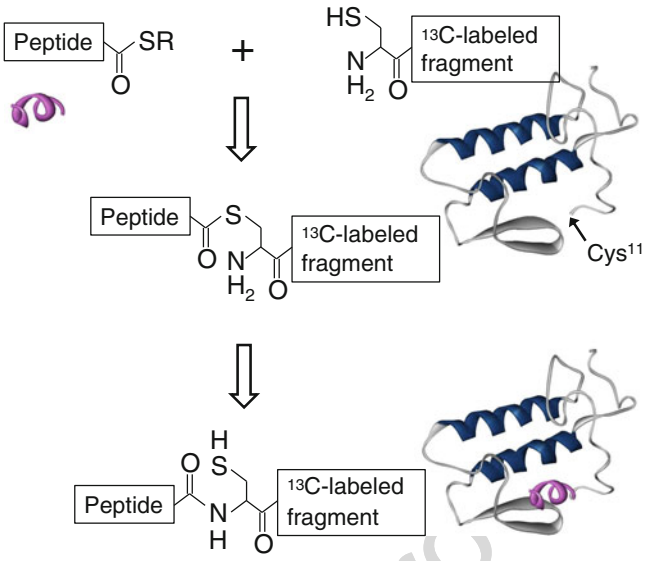

Fig. 6. Schematic description of production of a semisynthetic, segmentally ^{13}C-labeled protein using thioester-to-cysteine peptide ligation. Details are described in the main text.

fragment and the N-terminal peptide were 16 and 1.6 mg/ml, respectively, approximately corresponding to a 1:1 molar ratio.

4. The reaction was allowed to proceed for 6 h at 37°C, followed by refolding of the ligated protein by dialysis against 25 mM Tris–HCl, 5 mM $CaCl_2$, 5 mM L-cysteine, and 0.9 M guanidinum–HCl (pH 8.0), at 4°C. In thioester-to-cysteine-type peptide ligation, the thioester reacts with the thiol of cysteine side chain, followed by irreversible S–N acyl transfer and formation of a native peptide bond. Internal cysteines of the protein can also react with the thioesterified peptide, but these reactions are reversible under appropriately selected reducing conditions.
5. The ligated protein was purified by a Mono Q 5/50 column equilibrated with 2.5 mM KCl and 20 mM diethanolamine (pH 9.0).
6. This was followed by dialysis against 150 mM KCl, 25 mM Tris–HCl (pH 7.4), and additional purification using a size-exclusion HiLoad Superdex-75 column.
7. PLA_2 activity was measured using diheptanoyl-thiophosphatidylcholine as a substrate, as described elsewhere (40).

The semisynthetic, segmentally ^{13}C-labeled PLA_2 was dissolved in a D_2O-based buffer containing 100 mM NaCl, 1 mM NaN_3, 1 mM EGTA, 50 mM Hepes (pD 7.4) and injected into an ATR cell containing a supported membrane composed of 80 % 1-palmitoyl-2-oleoyl-*sn*-glycero-3-phosphocholine (POPC) and

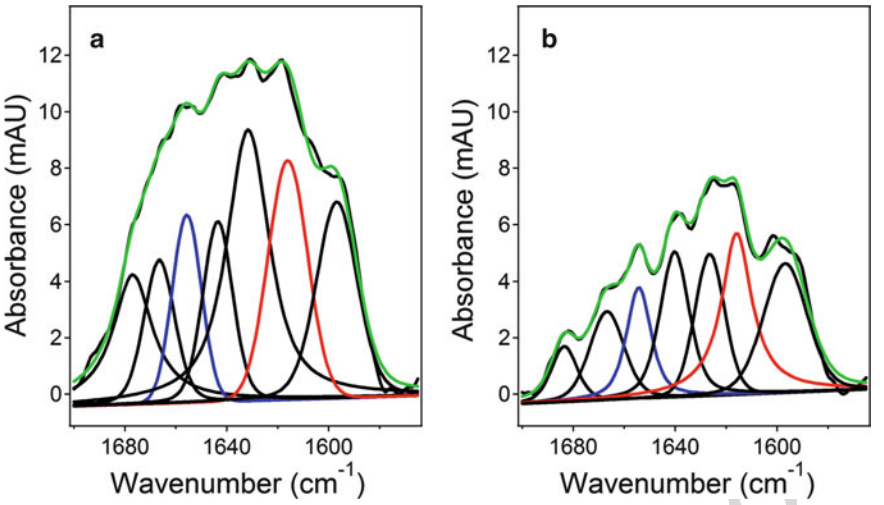

Fig. 7. ATR-FTIR spectra of a semisynthetic human pancreatic PLA_2 in which the N-terminal helix is unlabeled while the rest is uniformly ^{13}C-labeled, at *p* and *s* polarizations (**a** and **b**, respectively). The protein is bound to a POPC/POPG (4:1) bilayer supported on a germanium IRE, in a buffer of 100 mM NaCl, 1 mM NaN_3, 1 mM EGTA, 50 mM Hepes, pD 7.4. The *green line* is the curvefit, that is, the sum of all amide I components shown under the spectrum. The *blue* and *red* components are assigned to unlabeled and ^{13}C-labeled α-helices. Details are described in the main text.

20 % 1-palmitoyl-2-oleoyl-*sn*-glycero-3-phosphoglycerol (POPG). Polarized ATR-FTIR spectra of the membrane-bound protein, presented in Fig. 7, indicate relatively broad and complex amide I contours, resulting from the unlabeled and ^{13}C-labeled segments of the proteins, each of which is undergoing amide HX following distinct kinetics. Amide I components located around 1,656 cm^{-1} and 1,616 cm^{-1} were assigned to the unlabeled (^{12}C) and ^{13}C-labeled α-helices of PLA_2. Intensities of these components at *p* and *s* polarizations of the infrared light were used to determine the orientations of the unlabeled and ^{13}C-labeled α-helices. The interhelical angle between the two internal helices of pancreatic PLA_2 were shown to be ~6 °, using an analytic geometry algorithm (87), indicating that the two internal helices could be considered as one in terms of helical orientation. Determination of orientations of the N-terminal and the internal helices with respect to the membrane by polarized ATR-FTIR, combined with homology modeling and fluorescence quenching experiments, allowed identification of the orientation and the depth of membrane insertion of the membrane-bound protein molecule (PDB entry 1YSK). Similar protein engineering techniques, including protein semisynthesis and segmental ^{13}C-labeling, were used to generate a chimeric PLA_2 where the N-terminal unlabeled helix of human group IIA PLA_2 was ligated to a ^{13}C-labeled pancreatic (group IB) PLA_2 fragment (34). ATR-FTIR studies on the chimeric PLA_2 elucidated the regulatory role of the N-terminal helix in PLA_2 membrane binding mode and activity.

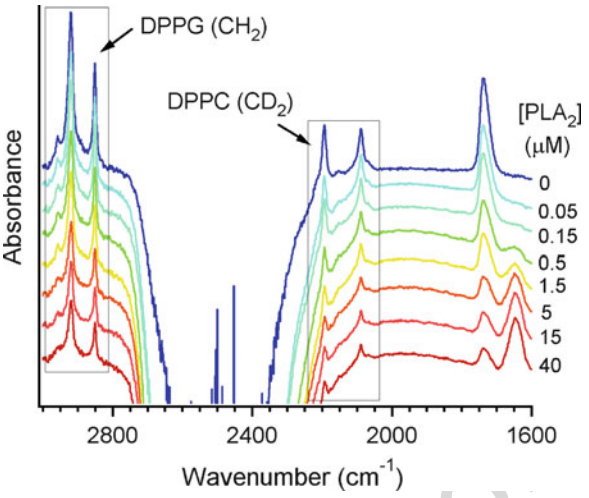

Fig. 8. ATR-FTIR spectra of a lipid bilayer composed of 50 % 1,2-(d_{62})dipalmitoyl-*sn*-glycero-3-phosphocholine (with deuterated acyl chains) and 50 % unlabeled 1,2-dipalmitoyl-*sn*-glycero-3-phosphoglycerol supported on a germanium IRE at various concentration of a snake venom PLA_2 in a buffer containing 2 mM $CaCl_2$. The CH_2 and CD_2 stretching vibrational bands of the unlabeled and deuterated lipids are shown in rectangular frames. Note the strong spectral downshift of methylene stretching vibrations upon deuteration, as well as the increase in protein amide I band (1,700–1,600 cm^{-1}) and the decrease in lipid methylene and carbonyl (~1,735 cm^{-1}) stretching bands with increasing PLA_2 concentration, indicating binding of PLA_2 to the supported membrane and lipid hydrolysis.

3.4.4. FTIR Studies on Isotopically Labeled Lipids

Isotope-edited FTIR spectroscopy has also been applied to study phase transitions, phase separation, hydration, and other properties of phospholipid membranes. Selective ^{13}C-labeling of lipid carbonyl groups at *sn*-1 or *sn*-2 positions identified their individual H-bonding and hydration properties and their contributions to the structure of the membrane–water interface (88–91). Deuteration of the methylene groups of lipid hydrocarbon chains results in ~730 cm^{-1} spectral downshift of the methylene stretching vibration, thus providing FTIR spectral resolution between unlabeled and deuterated lipids or between two chains of the same, selectively deuterated lipid. This effect was used to gain structural information on individual components of the membrane and the effect of membrane structure on membrane-bound enzyme activity (92–97). For example, lipid phase separation was found to promote protein kinase C activity (92). ATR-FTIR experiments on the action of PLA_2 on membranes composed of unlabeled and acyl chain deuterated lipids showed that (a) increased catalytic activity of PLA_2 toward negatively charged lipid membranes results from stronger membrane binding rather than selectivity for anionic lipids and (b) lipid hydrolysis is followed by preferential dissociation of the lyso-lipids and accumulation of free fatty acids in the membrane, which modulates the membrane charge and the morphology and thereby PLA_2 activity (ref. (13) and Fig. 8).

3.5. Conclusions and Perspectives

FTIR spectroscopy is a capable yet relatively easy biophysical technique to gain structural information on proteins and peptides. Studies on membrane proteins reconstituted in detergent micelles or lipid vesicles allow structural characterization of both the protein and the lipid, without any problems related to the molecular size or light scattering like in NMR or UV spectroscopy. While FTIR does not provide the atomic structures of molecules, it is highly sensitive to protein conformational changes, structural flexibility, and solvent accessibility. For example, differences between very similar structures such as α_I and α_{II} helices, which mainly differ by helical H-bonding strength, can be identified easily based on significant differences in vibrational frequencies of the two structures (6, 98). Polarized ATR-FTIR is especially well suited for studies on membrane-bound proteins and provides the protein's orientation with respect to the membrane in addition to protein secondary structure and the kinetics of amide HX. While significant progress has been made in site-directed structural analysis of proteins and peptides by isotope-edited FTIR, still both the theory and the experimental techniques need to be developed to a higher level. Complete understanding and structural interpretation of the spectra of isotope-labeled proteins and peptides requires a stringent theoretical framework of vibrational coupling between various amide modes and its relation to secondary and tertiary structure of the protein. Combination of protein engineering techniques, including peptide ligation, nonsense suppression, and other procedures, with FTIR spectroscopy, is one of the strategies that can break new ground in the whole field of structural biology.

4. Notes

In most studies, the secondary structures of proteins or peptides are estimated by curve-fitting of the amide I band assuming equal molar absorptivities (extinction coefficients) for all secondary structure types. While this may be an acceptable approximation, more accurate data may be obtained when the curve-fitting is conducted using the individual amide I extinction coefficients of various secondary structures. No consensus has been reached thus far regarding the quantitative determination of their values, however. Table 3 presents the values of extinction coefficients determined by Venyaminov and Kalnin (99), which are widely accepted and considered reliable. Jackson et al. (100) evaluated the following relative molar absorptivities of poly-L-lysine at different conformations: 1.00/1.16/0.88 for α-helix/β-sheet/random structure, respectively. De Jongh et al. (101) reported the relative extinction coefficients for α-helix (1.00), β-sheet (1.44–1.57), β-turns (0.48–0.75), and random structure (0.54–0.58). These estimates were derived from

comparison of FTIR amide I bands of 15 proteins, deposited on a germanium plate from an H_2O buffer and dried, with their structures determined by X-ray crystallography or NMR. Vedantham et al. (3) reported the wavenumbers, relative extinction coefficients, and bandwidths at half height for proteins in H_2O solutions. Based on these data, the peak absorbance and integrated extinction coefficients are calculated using the α-helical extinction coefficients reported in ref. (99) (Table 6). The relative extinction coefficients of various secondary structures are sufficient to determine the relative contents of secondary structures in a protein, which is the most useful information derived from FTIR, implying that the absolute values of the extinction coefficients are not needed to gain this information. Still there are significant differences in reported relative absorptivities, such as $\varepsilon_\alpha/\varepsilon_\beta \approx 1.0/1.5$ according to Venyaminov and Kalnin (99) and de Jongh et al. (101) vs. $\varepsilon_\alpha/\varepsilon_\beta \approx 1.0/0.8$ according to Vedantham et al. (3). More systematic studies are needed to resolve these differences.

Amide I frequencies of various secondary structures can vary depending on numerous factors, including the polypeptide chain length, environment, rigidity, etc. For example, the amide I wavenumbers of poly-L-lysine in α-helical and β-sheet, and random conformations in D_2O were 1,638 cm^{-1}, 1,610 cm^{-1} plus a weaker component at 1,680 cm^{-1}, and 1,644 cm^{-1} (100). It is possible that homopolypeptides generate lower amide I vibrational frequencies than proteins (i.e., heteropolypeptides) because of more regular secondary structures, corresponding to stronger H-bonding and hence weaker C=O bonds. Also, there may be significant overlap between different structures in the amide I region, as seen from Table 2.

Acknowledgments

Experimental data presented in this article have been obtained and published elsewhere by Kathleen N. Nemec, Shan Qin, Abhay H. Pande, and Pranav Garg.

References

1. Krimm S, Bandekar J (1986) Vibrational spectroscopy and conformation of peptides, polypeptides and proteins. Adv Protein Chem 38:181–364
2. Brauner JW, Dugan C, Mendelsohn R (2000) ^{13}C isotope labeling of hydrophobic peptides. Origin of the anomalous intensity distribution in the infrared amide I spectral region of β-sheet structures. J Am Chem Soc 122:677–683
3. Vedantham G, Sparks HG, Sane SU, Tzannis S, Przybycien TM (2000) A holistic approach for protein secondary structure estimation from infrared spectra in H_2O solutions. Anal Biochem 285:33–49

4. Hsu SL, Moore WH, Krimm S (1976) Vibrational spectrum of the unordered polypeptide chain: a Raman study of feather keratin. Biopolymers 15:1513–1528
5. Naik VM (1992) Vibrational spectroscopic studies of L, D-alternating valine peptides. Vib Spectrosc 3:105–113
6. Barnett SM, Edwards CM, Butler IS, Levin IW (1997) Pressure-induced transmembrane α_{II}- to α_I-helical conversion in bacteriorhodopsin: an infrared spectroscopic study. J Phys Chem B 101:9421–9424
7. Tamm LK, Tatulian SA (1997) Infrared spectroscopy of proteins and peptides in lipid bilayers. Q Rev Biophys 30:365–429
8. Fringeli UP (1993) *In situ* infrared attenuated total reflection membrane spectroscopy. In: Mirabella FM Jr (ed) Internal reflection spectroscopy. Theory and applications. Marcel Dekker, New York, pp 255–324
9. Fringeli UP, Günthard HH (1981) Infrared membrane spectroscopy. In: Grell E (ed) Membrane spectroscopy. Springer, Berlin, pp 270–332
10. Venyaminov SY, Prendergast FG (1997) Water (H_2O and D_2O) molar absorptivity in the 1000–4000 cm^{-1} range and quantitative infrared spectroscopy of aqueous solutions. Anal Biochem 248:234–245
11. Arrondo JLR, Goñi FM (1993) Infrared spectroscopic studies of lipid-protein interactions in membranes. In: Watts A (ed) Protein-lipid interactions. Elsevier Science Publishers B.V, Amsterdam, pp 321–349
12. Tatulian SA (2003) Attenuated total reflection Fourier transform infrared spectroscopy: a method of choice for studying membrane proteins and lipids. Biochemistry 42:11898–11907
13. Tatulian SA (2001) Toward understanding interfacial activation of secretory phospholipase A_2 (PLA_2): Membrane surface properties and membrane-induced structural changes in the enzyme contribute synergistically to PLA_2 activation. Biophys J 80:789–800
14. Tatulian SA, Cortes DM, Perozo E (1998) Structural dynamics of the *Streptomyces lividans* K^+ channel (SKC1): secondary structure characterization from FTIR spectroscopy. FEBS Lett 423:205–212
15. Tatulian SA, Tamm LK (2000) Secondary structure, orientation, oligomerization, and lipid interactions of the transmembrane domain of influenza hemagglutinin. Biochemistry 39:496–507
16. Tatulian SA (2003) Structural effects of covalent inhibition of phospholipase A_2 suggest allosteric coupling between membrane binding and catalytic sites. Biophys J 84:1773–1783
17. Tatulian SA, Biltonen RL, Tamm LK (1997) Structural changes in a secretory phospholipase A_2 induced by membrane binding: a clue to interfacial activation? J Mol Biol 268:809–815
18. Pande AH, Moe D, Nemec KN, Qin S, Tan S, Tatulian SA (2004) Modulation of human 5-lipoxygenase activity by membrane lipids. Biochemistry 43:14653–14666
19. Tatulian SA, Qin S, Pande AH, He X (2005) Positioning membrane proteins by novel protein engineering and biophysical approaches. J Mol Biol 351:939–947
20. Glasoe PK, Long FA (1960) Use of glass electrodes to measure acidities in deuterium oxide. J Phys Chem 64:188–190
21. Makhatadze GI, Clore GM, Gronenborn AM (1995) Solvent isotope effect and protein stability. Nat Struct Biol 2:852–855
22. Nemec KN, Pande AH, Qin S, Bieber Urbauer RJ, Tan S, Moe D, Tatulian SA (2006) Structural and functional effects of tryptophans inserted into the membrane-binding and substrate-binding sites of human group IIA phospholipase A_2. Biochemistry 45:12448–12460
23. Marley J, Lu M, Bracken C (2001) A method for efficient isotope labeling of recombinant proteins. J Biomol NMR 20:71–75
24. Hill JM (2008) NMR screening for rapid protein characterization in structural proteomics. Methods Mol Biol 426:437–446
25. Kandori H, Nakamura H, Yamazaki Y, Mogi T (2005) Redox-induced protein structural changes in cytochrome *bo* revealed by Fourier transform infrared spectroscopy and [^{13}C]Tyr Labeling. J Biol Chem 280:32821–32826
26. Cheong JJ, Hwang I, Rhee S, Moon TW, Choi YD, Kwon HB (2007) Complementation of an *E. coli* cysteine auxotrophic mutant for the structural modification study of 3'(2'),5'-bisphosphate nucleotidase. Biotechnol Lett 29:913–918
27. Strømgaard A, Jensen AA, Strømgaard K (2004) Site-specific incorporation of unnatural amino acids into proteins. Chembiochem 5:909–916
28. Hendrickson TL, de Crécy-Lagard V, Schimmel P (2004) Incorporation of nonnatural amino acids into proteins. Annu Rev Biochem 73:147–176
29. Xie J, Schultz PG (2005) Adding amino acids to the genetic repertoire. Curr Opin Chem Biol 9:548–554

30. Seyedsayamdost MR, Stubbe J (2009) Replacement of Y_{730} and Y_{731} in the α2 subunit of *Escherichia coli* ribonucleotide reductase with 3-aminotyrosine using an evolved suppressor tRNA/tRNA-synthetase pair. Methods Enzymol 462:45–76
31. Liu CC, Schultz PG (2010) Adding new chemistries to the genetic code. Annu Rev Biochem 79:413–444
32. Anderson RD 3rd, Zhou J, Hecht SM (2002) Fluorescence resonance energy transfer between unnatural amino acids in a structurally modified dihydrofolate reductase. J Am Chem Soc 124:9674–9675
33. Sisido M, Ninomiya K, Ohtsuki T, Hohsaka T (2005) Four-base codon/anticodon strategy and non-enzymatic aminoacylation for protein engineering with non-natural amino acids. Methods 36:270–278
34. Qin S, Pande AH, Nemec KN, He X, Tatulian SA (2005) Evidence for the regulatory role of the N-terminal helix of secretory phospholipase A_2 from studies on native and chimeric proteins. J Biol Chem 280:36773–36783
35. Venyaminov SY, Hedstrom JF, Prendergast FG (2001) Analysis of the segmental stability of helical peptides by isotope-edited infrared spectroscopy. Proteins 45:81–89
36. Huang R, Kubelka J, Barber-Armstrong W, Silva RA, Decatur SM, Keiderling TA (2004) Nature of vibrational coupling in helical peptides: an isotopic labeling study. J Am Chem Soc 126:2346–2354
37. Petty SA, Decatur SM (2005) Intersheet rearrangement of polypeptides during nucleation of β-sheet aggregates. Proc Natl Acad Sci U S A 102:14272–14277
38. Ramajo AP, Petty SA, Starzyk A, Decatur SM, Volk M (2005) The α-helix folds more rapidly at the C-terminus than at the N-terminus. J Am Chem Soc 127:13784–13785
39. Lewis RN, McElhaney RN (2009) The physicochemical properties of cardiolipin bilayers and cardiolipin-containing lipid membranes. Biochim Biophys Acta 1788:2069–2079
40. Qin S, Pande AH, Nemec KN, Tatulian SA (2004) The N-terminal α-helix of pancreatic phospholipase A_2 determines productive-mode orientation of the enzyme at the membrane surface. J Mol Biol 344:71–89
41. Pande AH, Qin S, Tatulian SA (2005) Membrane fluidity is a key modulator of membrane binding, insertion, and activity of 5-lipoxygenase. Biophys J 88:4084–4094
42. Renthal R (2006) An unfolding story of helical transmembrane proteins. Biochemistry 45:14559–14566
43. Sanders CR, Sönnichsen F (2006) Solution NMR of membrane proteins: practice and challenges. Magn Reson Chem 44:S24–S40
44. Vinogradova O, Sönnichsen F, Sanders CR 2nd (1998) On choosing a detergent for solution NMR studies of membrane proteins. J Biomol NMR 11:381–386
45. Tatulian SA, Hinterdorfer P, Baber G, Tamm LK (1995) Influenza hemagglutinin assumes a tilted conformation during membrane fusion as determined by attenuated total reflection FTIR spectroscopy. EMBO J 14:5514–5523
46. Tatulian SA, Chen B, Li J, Negash S, Middaugh CR, Bigelow DJ, Squier TC (2002) The inhibitory action of phospholamban involves stabilization of α-helices within the Ca^{2+}-ATPase. Biochemistry 41:741–751
47. Axelsen PH, Citra MJ (1996) Orientational order determination by internal reflection infrared spectroscopy. Prog Biophys Mol Biol 66:227–253
48. Goormaghtigh E, Raussens V, Ruysschaert JM (1999) Attenuated total reflection infrared spectroscopy of proteins and lipids in biological membranes. Biochim Biophys Acta 1422:105–185
49. Silvestro L, Axelsen PH (2000) Membrane-induced folding of cecropin A. Biophys J 79:1465–1477
50. Citra MJ, Axelsen PH (1996) Determination of molecular order in supported lipid membranes by internal reflection Fourier transform infrared spectroscopy. Biophys J 71:1796–1805
51. Silvestro L, Axelsen PH (1999) Fourier transform infrared linked analysis of conformational changes in annexin V upon membrane binding. Biochemistry 38:113–121
52. Vigano C, Goormaghtigh E, Ruysschaert JM (2003) Detection of structural and functional asymmetries in P-glycoprotein by combining mutagenesis and H/D exchange measurements. Chem Phys Lipids 122:121–135
53. Beevers AJ, Kukol A (2006) The transmembrane domain of the oncogenic mutant ErbB-2 receptor: a structure obtained from site-specific infrared dichroism and molecular dynamics. J Mol Biol 361:945–953
54. Marsh D, Müller M, Schmitt F-J (2000) Orientation of the infrared transition moments for an α-helix. Biophys J 78:2499–2510
55. Marsh D, Páli T (2001) Infrared dichroism from the X-ray structure of bacteriorhodopsin. Biophys J 80:305–312

56. Páli T, Marsh D (2001) Tilt, twist, and coiling in β-barrel membrane proteins: relation to infrared dichroism. Biophys J 80:2789–2797
57. Harrick NJ (1987) Internal reflection spectroscopy. Harrick Scientific Corporation, Ossining, NY
58. Marsh D (2000) Infrared dichroism of twisted β-sheet barrels. The structure of *E. coli* outer membrane proteins. J Mol Biol 297:803–808
59. Marsh D (1999) Quantitation of secondary structure in ATR infrared spectroscopy. Biophys J 77:2630–2637
60. Arkin IT (2006) Isotope-edited IR spectroscopy for the study of membrane proteins. Curr Opin Chem Biol 10:394–401
61. Decatur SM (2006) Elucidation of residue-level structure and dynamics of polypeptides via isotope-edited infrared spectroscopy. Acc Chem Res 39:169–175
62. Flach CR, Cai P, Dieudonné D, Brauner JW, Keough KM, Stewart J, Mendelsohn R (2003) Location of structural transitions in an isotopically labeled lung surfactant SP-B peptide by IRRAS. Biophys J 85:340–349
63. Paul C, Wang J, Wimley WC, Hochstrasser RM, Axelsen PH (2004) Vibrational coupling, isotopic editing, and β-sheet structure in a membrane-bound polypeptide. J Am Chem Soc 126:5843–5850
64. Tatulian SA (2010) Structural analysis of proteins by isotope-edited FTIR spectroscopy. Spectroscopy Int J 24:37–43
65. Barber-Armstrong W, Donaldson T, Wijesooriya H, Silva RA, Decatur SM (2004) Empirical relationships between isotope-edited IR spectra and helix geometry in model peptides. J Am Chem Soc 126:2339–2345
66. Ludlam CF, Arkin IT, Liu XM, Rothman MS, Rath P, Aimoto S, Smith SO, Engelman DM, Rothschild KJ (1996) Fourier transform infrared spectroscopy and site-directed isotope labeling as a probe of local secondary structure in the transmembrane domain of phospholamban. Biophys J 70:1728–1736
67. Arkin IT, MacKenzie KR, Brünger AT (1997) Site-directed dichroism as a method for obtaining rotational and orientational constraints for oriented polymers. J Am Chem Soc 119:8973–8980
68. Marsh D (2004) Infrared dichroism of isotope-edited α-helices and β-sheets. J Mol Biol 338:353–367
69. Torres J, Adams PD, Arkin IT (2000) Use of a new label, $^{13}C{=}^{18}O$, in the determination of a structural model of phospholamban in a lipid bilayer. Spatial restraints resolve the ambiguity arising from interpretations of mutagenesis data. J Mol Biol 300:677–685
70. Torres J, Kukol A, Goodman JM, Arkin IT (2001) Site-specific examination of secondary structure and orientation determination in membrane proteins: the peptidic $^{13}C{=}^{18}O$ group as a novel infrared probe. Biopolymers 59:396–401
71. Kukol A, Torres J, Arkin IT (2002) A structure for the trimeric MHC class II-associated invariant chain transmembrane domain. J Mol Biol 320:1109–1117
72. Brewer SH, Song B, Raleigh DP, Dyer RB (2007) Residue specific resolution of protein folding dynamics using isotope-edited infrared temperature jump spectroscopy. Biochemistry 46:3279–3285
73. Amunson KE, Ackels L, Kubelka J (2008) Site-specific unfolding thermodynamics of a helix-turn-helix protein. J Am Chem Soc 130:8146–8147
74. Londergan CH, Wang J, Axelsen PH, Hochstrasser RM (2006) Two-dimensional infrared spectroscopy displays signatures of structural ordering in peptide aggregates. Biophys J 90:4672–4685
75. Kim YS, Liu L, Axelsen PH, Hochstrasser RM (2008) Two-dimensional infrared spectra of isotopically diluted amyloid fibrils from Abeta40. Proc Natl Acad Sci U S A 105:7720–7725
76. Kim YS, Liu L, Axelsen PH, Hochstrasser RM (2009) 2D IR provides evidence for mobile water molecules in beta-amyloid fibrils. Proc Natl Acad Sci U S A 106:17751–17756
77. Shim SH, Gupta R, Ling YL, Strasfeld DB, Raleigh DP, Zanni MT (2009) Two-dimensional IR spectroscopy and isotope labeling defines the pathway of amyloid formation with residue-specific resolution. Proc Natl Acad Sci U S A 106:6614–6619
78. Zanni MT, Hochstrasser RM (2001) Two-dimensional infrared spectroscopy: a promising new method for the time resolution of structures. Curr Opin Struct Biol 11:516–522
79. Haris PI, Robillard GT, van Dijk AA, Chapman D (1992) Potential of ^{13}C and ^{15}N labeling for studying protein-protein interactions using Fourier transform infrared spectroscopy. Biochemistry 31:6279–6284
80. Zhang M, Fabian H, Mantsch HH, Vogel HJ (1994) Isotope-edited Fourier transform infrared spectroscopy studies of calmodulin's interaction with its target peptides. Biochemistry 33:10883–10888

81. Das KP, Choo-Smith LP, Petrash JM, Surewicz WK (1999) Insight into the secondary structure of non-native proteins bound to a molecular chaperone α-crystallin. An isotope-edited infrared spectroscopic study. J Biol Chem 274:33209–33212
82. Haris PI (2010) Can infrared spectroscopy provide information on protein-protein interactions? Biochem Soc Trans 38:940–946
83. Tam JP, Yu Q, Miao Z (1999) Orthogonal ligation strategies for peptide and protein. Biopolymers 51:311–332
84. Camarero JA, Muir TW (2001) Native chemical ligation of polypeptides. Curr Protoc Protein Sci Ch. 18:Unit18.4
85. Muralidharan V, Muir TW (2006) Protein ligation: an enabling technology for the biophysical analysis of proteins. Nat Methods 3:429–438
86. Muir TW (2008) Studying protein structure and function using semisynthesis. Biopolymers 90:743–750
87. Tatulian SA (2008) Determination of helix orientations in proteins. Comput Biol Chem 32:370–374
88. Blume A, Hübner W, Messner G (1988) Fourier transform infrared spectroscopy of $^{13}C{=}O$-labeled phospholipids hydrogen bonding to carbonyl groups. Biochemistry 27:8239–8249
89. Hübner W, Mantsch HH, Paltauf F, Hauser H (1994) Conformation of phosphatidylserine in bilayers as studied by Fourier transform infrared spectroscopy. Biochemistry 33:320–326
90. Lewis RN, McElhaney RN (1993) Studies of mixed-chain diacyl phosphatidylcholines with highly asymmetric acyl chains: a Fourier transform infrared spectroscopic study of interfacial hydration and hydrocarbon chain packing in the mixed interdigitated gel phase. Biophys J 65:1866–1877
91. Lewis RN, McElhaney RN, Pohle W, Mantsch HH (1994) Components of the carbonyl stretching band in the infrared spectra of hydrated 1,2-diacylglycerolipid bilayers: a reevaluation. Biophys J 67:2367–2375
92. Dibble AR, Hinderliter AK, Sando JJ, Biltonen RL (1996) Lipid lateral heterogeneity in phosphatidylcholine/phosphatidylserine/diacylglycerol vesicles and its influence on protein kinase C activation. Biophys J 71:1877–1890
93. Moore DJ, Gioioso S, Sills RH, Mendelsohn R (1999) Some relationships between membrane phospholipid domains, conformational order, and cell shape in intact human erythrocytes. Biochim Biophys Acta 1415:342–348
94. Binder H, Gawrisch K (2001) Dehydration induces lateral expansion of polyunsaturated 18:0–22:6 phosphatidylcholine in a new lamellar phase. Biophys J 81:969–982
95. Mimeault M, Bonenfant D (2002) FTIR spectroscopic analyses of the temperature and pH influences on stratum corneum lipid phase behaviors and interactions. Talanta 56:395–405
96. Fidorra M, Heimburg T, Seeger HM (2009) Melting of individual lipid components in binary lipid mixtures studied by FTIR spectroscopy, DSC and Monte Carlo simulations. Biochim Biophys Acta 1788:600–607
97. Gorcea M, Hadgraft J, Moore DJ, Lane ME (2011) Fourier transform infrared spectroscopy studies of lipid domain formation in normal and ceramide deficient stratum corneum lipid models. Int J Pharm. doi:10.1016/j.ijpharm.2011.11.004
98. Dwivedi AM, Krimm S (1984) Vibrational analysis of peptides, polypeptides, and proteins. XVIII. Conformational sensitivity of the alpha-helix spectrum: alpha I- and alpha II-poly(L-alanine). Biopolymers 23:923–943
99. Venyaminov SY, Kalnin NN (1990) Quantitative IR spectrophotometry of peptide compounds in water (H_2O) solutions. II. Amide absorption bands of polypeptides and fibrous proteins in α-, β-, and random coil conformations. Biopolymers 30:1259–1271
100. Jackson M, Haris PI, Chapman D (1989) Conformational transitions in poly(L-lysine): studies using Fourier transform infrared spectroscopy. Biochim Biophys Acta 998:75–79
101. de Jongh HH, Goormaghtigh E, Ruysschaert JM (1996) The different molar absorptivities of the secondary structure types in the amide I region: an attenuated total reflection infrared study on globular proteins. Anal Biochem 242:95–103
102. Stuart B (1997) Biological applications of infrared spectroscopy. Wiley, Chichester
103. Némethy G, Phillips DC, Leach SJ, Scheraga HA (1967) A second right-handed helical structure with the parameters of the Pauling-Corey α-helix. Nature 214:363–365
104. Heimburg T, Schuenemann J, Weber K, Geisler N (1996) Specific recognition of coiled coils by infrared spectroscopy: analysis of the three structural domains of type III intermediate filament proteins. Biochemistry 35:1375–1382
105. Reisdorf WC, Krimm S (1996) Infrared amide I' band of the coiled coil. Biochemistry 35:1383–1386

106. Kennedy DF, Crisma M, Toniolo C, Chapman D (1991) Studies of peptides forming 3_{10}- and α-helices and beta-bend ribbon structures in organic solution and in model biomembranes by Fourier transform infrared spectroscopy. Biochemistry 30:6541–6548

107. Martinez G, Millhauser G (1995) FTIR spectroscopy of alanine-based peptides: assignment of the amide I' modes for random coil and helix. J Struct Biol 114:23–27

108. Miick SM, Martinez GV, Fiori WR, Todd AP, Millhauser GL (1992) Short alanine-based peptides may form 3_{10}-helices and not α-helices in aqueous solution. Nature 359:653–655

109. Naik VM, Krimm S (1986) Vibrational analysis of the structure of gramicidin A. I. Normal mode analysis. Biophys J 49:1131–1145

110. Naik VM, Krimm S (1986) Vibrational analysis of the structure of gramicidin A. II. Vibrational spectra. Biophys J 49:1147–1154

111. Jackson M, Mantsch HH (1995) The use and misuse of FTIR spectroscopy in the determination of protein structure. Crit Rev Biochem Mol Biol 30:95–120

112. Papanikolopoulou K, Mills-Henry I, Thol SL, Wang Y, Gross AA, Kirschner DA, Decatur SM, King J (2008) Formation of amyloid fibrils in vitro by human γD-crystallin and its isolated domains. Mol Vis 14:81–89

113. Itkin A, Dupres V, Dufrêne YF, Bechinger B, Ruysschaert JM, Raussens V (2011) Calcium ions promote formation of amyloid β-peptide (1–40) oligomers causally implicated in neuronal toxicity of Alzheimer's disease. PLoS One 6:e18250

114. Karjalainen EL, Ravi HK, Barth A (2011) Simulation of the amide I absorption of stacked β-sheets. J Phys Chem B 115:749–757

115. Pauling L, Corey RB (1951) The pleated sheet, a new layer configuration of polypeptide chains. Proc Natl Acad Sci U S A 37:251–256

116. Armen RS, DeMarco ML, Alonso DO, Daggett V (2004) Pauling and Corey's α-pleated sheet structure may define the prefibrillar amyloidogenic intermediate in amyloid disease. Proc Natl Acad Sci U S A 101:11622–11627

117. Daggett V (2006) Alpha-sheet: the toxic conformer in amyloid diseases? Acc Chem Res 39:594–602

118. Wu H, Canfield A, Adhikari J, Huo S (2010) Quantum mechanical studies on model α-pleated sheets. J Comput Chem 31:1216–1223

119. Venyaminov SY, Kalnin NN (1990) Quantitative IR spectrophotometry of peptide compounds in water (H_2O) solutions. I. Spectral parameters of amino acid residue absorption bands. Biopolymers 30:1243–1257

120. Chirgadze YN, Fedorov OV, Trushina NP (1975) Estimation of amino acid residue side-chain absorption in the infrared spectra of protein solutions in heavy water. Biopolymers 14:679–694

Author Queries

Chapter No.: 9 214093_1_En

Query Refs.	Details Required	Author's response
AU1	The Fig. [9.5] has to be printed in black but color is mentioned in the caption. Please amend the caption accordingly.	